

# Snapshotting the transient conformation and tracing the multiple pathways of single peptides folding using solid-state nanopore

Shao-Chuang Liu<sup>a,b</sup>, Yi-Lun Ying<sup>a</sup>, Wei-Hua Li<sup>c</sup>, Yong-Jing Wan<sup>d</sup>, Yi-Tao Long<sup>\*a,b</sup>

<sup>a</sup> State Key Laboratory of Analytical Chemistry for Life Science, School of Chemistry and Chemical Engineering, Nanjing University, Nanjing, 210023, P.R. China.

<sup>b</sup> Department of Chemistry, East China University of Science and Technology, Shanghai 200237, P. R. China.

<sup>c</sup> Shanghai Key Laboratory of New Drug Design, School of Pharmacy, East China University of Science and Technology, Shanghai 200237, P. R. China.

<sup>d</sup> School of Information Science and Engineering, East China University of Science and Technology, Shanghai 200237, P.R. China.

\* To whom correspondence should be addressed: [yitaolong@nju.edu.cn](mailto:yitaolong@nju.edu.cn)

## Contents

1	Experimental Procedures.....	3
1.1	Materials.....	3
1.2	Preparation of biotinylated peptide –monovalent streptavidin complex.....	3
1.3	Nanopore fabrication.....	3
1.4	Nanopore experimental methods.....	4
1.5	Data analysis.....	4
1.6	Markov chain modeling.....	5
1.7	Molecular dynamics simulation.....	5
2	Results and Discussion.....	7
2.1	Control experiment of $\beta$ -hairpin peptide and monovalent streptavidin detection.....	7
2.2	Raw current trace of the peptide-mSA complex detection with different voltage.....	8
2.3	The scatter plots and time probability of the example signals for the four kinds of typical current patterns.....	9
2.4	The confined effects on the time probability of single $\beta$ -hairpin for each current stage.....	9
2.5	Sequence .dependent conformational dynamics of single $\beta$ -hairpin.....	10
2.6	Current histogram of single peptide events with $d \sim 4$ nm nanopore under +100 mV.....	11
2.7	Current histogram of single peptide events with $d \sim 4$ nm nanopore under +150 mV.....	17
2.8	Current histogram of single peptide events with $d \sim 4$ nm nanopore under +200 mV.....	23

2.9	Current histogram of single peptide events with $d \sim 5$ nm nanopore under +50 mV.....	29
2.10	Current histogram of single peptide events with $d \sim 5$ nm nanopore under +100 mV. ....	31
2.11	Current histogram of single peptide events with $d \sim 5$ nm nanopore under +150 mV. ....	33

## 1 Experimental Procedures

### 1.1 Materials.

The peptide is purchased from Sangon Biotech (Shanghai) Co., Ltd and GL Biochem (Shanghai) Ltd with HPLC analysis and purification. The sequence of the  $\beta$ -hairpin peptide is shown in Figure S1 from the C-terminal fragment (41-56) of protein G B1 domain (PDB code: 1GB1). The  $11.4 \pm 2.5$  nm thin free-standing Silicon nitride (SiNx) membrane with  $50 \mu\text{m} \times 50 \mu\text{m}$  window size is purchased from Norcada Inc., CAN (Norcada product #NT005Z). The nanopores used to obtain TEM images were fabricated in  $14.9 \pm 2.5$  nm thick membranes with windows size of  $10 \mu\text{m} \times 10 \mu\text{m}$  (Norcada product #L15). A high-resolution transmission electron microscopy (JEM-2100, JEOL Inc., USA) was operated at an accelerating voltage of 200 kV to obtain the TEM images. Potassium chloride (KCl,  $\geq 99.5\%$ ) was purchased from Sigma-Aldrich (St. Louis, MO, USA). Tris (hydroxymethyl) aminomethane (Tris,  $\geq 99.9\%$ ) was purchased from Aladdin Reagent Co., Ltd. (Shanghai, China). Sodium phosphate monobasic ( $\text{NaH}_2\text{PO}_4$ , 99%), sodium phosphate dibasic ( $\text{Na}_2\text{HPO}_4$ , 99%), sodium chloride (NaCl, 99%), potassium phosphate monobasic ( $\text{KH}_2\text{PO}_4$ ) were purchased from Shanghai Lingfeng Chemical Reagent Co., Ltd. (Shanghai, China). The monovalent streptavidin is a gift from Prof. Mark Howarth at Oxford University.<sup>1</sup> All reagents were of analytical grade. All solutions were prepared by Milli-Q ultrapure water with the resistance of  $18.2 \text{ M } \Omega \text{ cm}$  at  $25 \text{ }^\circ\text{C}$  (EMD Millipore, Billerica, USA) and were filtered with  $0.22 \mu\text{m}$  pore-size filter (Rephile Bioscience Ltd., Shanghai, China).

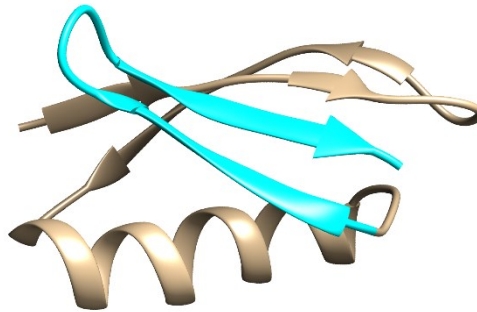


**Figure S1.** The structure of the B1 domain of protein G (PDB code: 1GB1). The cyan color indicates the  $\beta$ -hairpin from the C-terminal fragment (41-56) used in this study.

### 1.2 Preparation of biotinylated peptide –monovalent streptavidin complex.

The  $\beta$ -hairpin peptide with biotin tags at the C terminus is dissolved in pH 7.4 PBS solution at a concentration of  $2 \mu\text{M}$ . The mSA protein is also diluted to  $2 \mu\text{M}$  with pH 7.4 PBS. Then equal molar peptide and mSA protein solution mixed at  $35 \text{ }^\circ\text{C}$  to ensure the peptide connects with the protein one to one adequately and forms an mSA-biotin-peptide complex. The native-PAGE analysis was used to confirm the biotinylate beta-hairpin is well bound connected with the mSA protein.

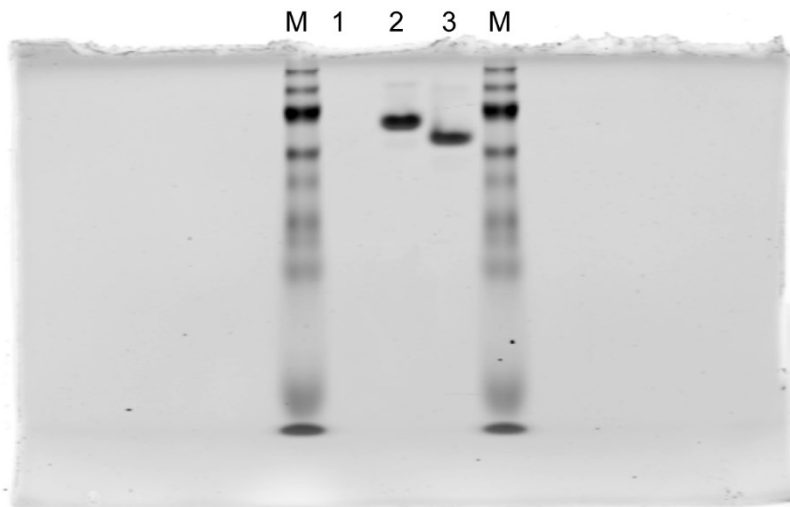


**Figure S2.** Native-PAGE identifying the binding between the mSA proteins and biotinylate beta-hairpin peptide. Molecule mass marker (M) and analysis of the following: (1) biotinylate beta-hairpin peptide; (2) free mSA protein; (3) mSA-biotin-peptide complex.

### 1.3 Nanopore fabrication.

The SiN<sub>x</sub> nanopore is fabricated by the method of dielectric breakdown according to the previous studies.<sup>1-3</sup> Briefly, a SiN<sub>x</sub> chip hydrophobically treated in piranha solutions and oxygen plasma. Then, the SiN<sub>x</sub> chip is placed in a custom polytetrafluoroethylene (PTFE) chamber to separate two 200-μL fluidic reservoirs as *cis* and *trans*, respectively. After, the chamber is filled with the ionic electrolyte solution (1 M KCl, 10 mM Tris-HCL, pH 8.0). Two Ag/AgCl electrodes were immersed on both sides of the chamber. The entire system is placed in a grounded Faraday cage to isolate it from electromagnetic interference. Voltage application and leakage current monitoring are used self-designed LabVIEW software to control custom-build current amplifiers with PCI-6251 DAQ card.<sup>1,2</sup> In the fabrication process, the value of the trans-membrane potential is set by the software and the leakage current will be acquired with 1 K sampling rate. When the leakage current exceeds the pre-set threshold, the voltage is terminated immediately by the software. After the fabrication, the chip was cleaned with ultra-pure waters at a high temperature of 80 °C several times to remove the contaminating salt presenting in the chips. Then, the TEM was used to locate the single pore from 10 μm × 10 μm membrane as well as take the TEM image. A high-resolution transmission electron microscopy (JEM-2100, JEOL Ltd., Japan) was operated at an accelerating voltage of 200 kV to obtain the TEM images.

Note that the size of the nanopore is confirmed by both the conductance calculation from the I-V curve and the TEM image (Figure 1a-1b and Figure S3). For example, the current-voltage (I-V) curve in Figure 1b yields the pore conductance *G* of 17.3 nS in 1 M KCl. Then, the effective diameter of the pore (*d*) could be calculated from its conductance *G* as follows:<sup>2,4,5</sup>

$$G = \sigma \left( \frac{4l}{\pi d^2} + \frac{1}{d} \right)^{-1} \quad (1)$$

where  $\sigma$  is the bulk conductivity of 1 M KCl (10.5 S m<sup>-1</sup>), and *l* is the effective thickness of the SiN<sub>x</sub> membrane. A previous study has demonstrated that the effective length of nanopores created by multi-level pulse-voltage injection is approximately one-third of the actual membrane thickness.<sup>6</sup> Since the membrane thickness is 11.4 ± 2.5 (Norcada product #NT005Z), the calculated pore diameter in Figure 1b is *d* = 3.8 nm from eq. (1) with *l* = 3.7 nm, which is comparable to the TEM image in Figure 1c. Figure S3 shows the I-V curves and TEM images of the SiN<sub>x</sub> nanopore used in our experiments.

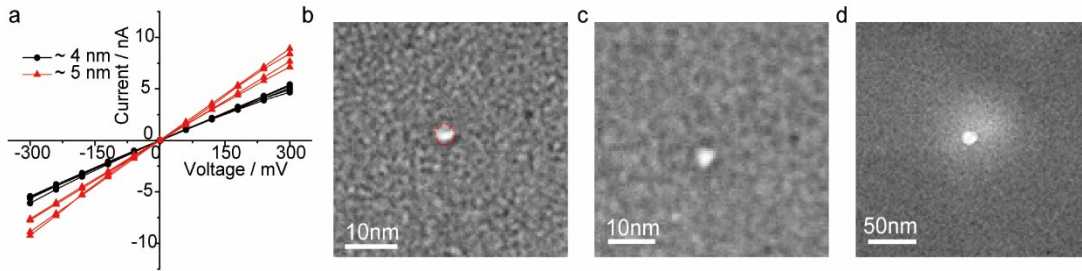


**Figure S3.** The I-V curve (a) and TEM (b-d) characterization of the SiN<sub>x</sub> nanopore.

#### 1.4 Nanopore experimental methods.

1 μL mSA-peptide complex solution was added into the *trans* side of the chamber with a final concentration of 5 nM in 1 M KCl, pH 8.0 (Figure 1). Current traces were measured at a sampling rate of 100 kHz using Axopatch 200B (Axon Instruments, Forest City, USA) with a 5 kHz low-pass Bessel filter. To ensure a high-throughput recording of the captured events, the data acquisition is performed in the episodic stimulation mode of the Axon Digidata 1550A system with 7 s positive potential of +150 mV to capture the mSA-peptide complex and 3 s negative potential of -200 mV to release it in each sweep. The total time of each sweep in this mode is 10 s under a sample rate of 100 kHz.

#### 1.5 Data analysis.

Data analysis was performed using a home-designed program based on our previous data recovery methods,<sup>7,8</sup> and the self-designed python program of PyNano.<sup>[9]</sup> The representative processing of the data is shown in Figure S4. To minimize the current evaluation error, we excluded an exceedingly short-lived spike with durations < 40 μs or 10 sample points. As shown in Figure S4, the black dotted plot is the raw data of one recorded event. The red line is the fitted result using the PyNano.<sup>9</sup> We define the current of baseline as *I*<sub>0</sub>, and the current of each spike as *I*<sub>*i*</sub> whereas *i* is the spike number in the whole event. Then, the current amplitude of each spike ( $\Delta I_i/I_0$ ) could be described as follows:

$$\frac{\Delta I_i}{I_0} = \frac{I_0 - I_i}{I_0} = 1 - \frac{I_i}{I_0} \quad (2)$$

The blue dots with enclosed numbers in Figure S4 define the duration value ( $\Delta t_i$ ) of each spike, whereas *i* is the spike number in the whole event. *t*<sub>0</sub> denotes the start time point for the entire event. Then,  $\Delta t_i$  of each spike could be described as follows:

$$\Delta t_i = t_i - t_{i-1} \quad (3)$$

The current histograms of all the  $\Delta I_i/I_0$  in each event were fitted to Gaussian functions while the duration histograms of all  $\Delta t_i$  in each event were fitted to exponential functions. After evaluating the current histogram of the spikes from all the events, we find that the current blockage of all the events has four main peaks. We use the peak center of the Gaussian fits as the center of the dominated stage. And the average peak width to set up the threshold of each stage. Then we could set the  $\Delta I_i/I_0$  values of every spike into four current stages.

The duration time probability ( $P_m$ ,  $n = 1, 2, 3$ , or  $4$ ) of each stage to the entire event duration could be calculated as follows:

$$P_{tn} = \frac{t_{sn}}{t_{s1} + t_{s2} + t_{s3} + t_{s4}} \times 100\% \quad (4)$$

Whereas  $t_{sn}$  ( $n = 1, 2, 3$  or  $4$ ) corresponds to the sum of spike durations at each current stage.

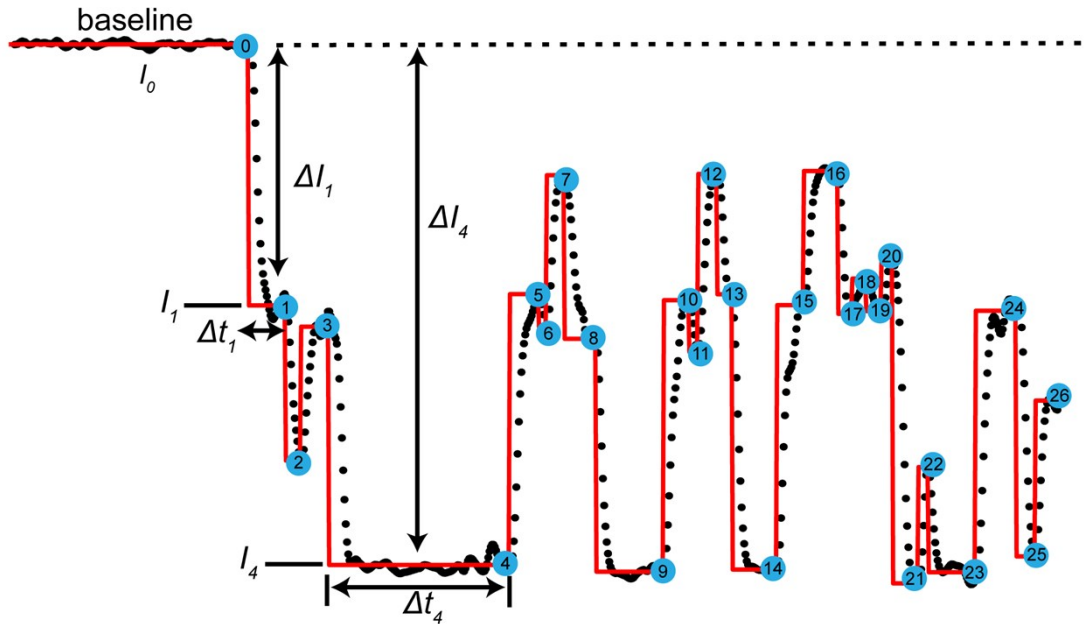


**Figure S4.** Evaluating the duration and current amplitude for each spike in the entire event. The dotted plot represents a raw current trace. The red line is the fitted data using the self-developed software of PyNano, which shows the trajectory for the event evaluation. The blue enclosed numbers illustrate the start point and endpoint of each blockage level. For example, the current amplitude and duration of spike 1 is  $\Delta I_1/I_0 = 1 - I_1/I_0$ , and  $\Delta t_1 = t_1 - t_0$  while those of spike 4 is  $\Delta I_4/I_0 = 1 - I_3/I_0$ , and  $\Delta t_4 = t_4 - t_3$ , respectively.

## 1.6 Markov chain modeling

Taking the +150 mV voltage as an example, we have observed for possible current stages, which assigned as stage 1 of  $\Delta I_i/I_0 = 0.1 - 0.24$ , stage 2 of  $\Delta I_i/I_0 = 0.24 - 0.46$ , stage 3 of  $\Delta I_i/I_0 = 0.46 - 0.58$  and stage 4  $\Delta I_i/I_0 = 0.58 - 0.8$ , respectively. The occur and transition of these four stages is random with different probability and can be described by a simple multi-state model known as a Markov chain in probability theory.<sup>10</sup> As shown in Figure S4, for stage 1, in a short period, it can transition to another permitted state of 2, 3, 4, or remain unchanged, which can be expressed by a probability matrix ( $P(n1 \rightarrow 1)$ ,  $P(n1 \rightarrow 2)$ ,  $P(n1 \rightarrow 3)$ ,  $P(n1 \rightarrow 4)$ ).

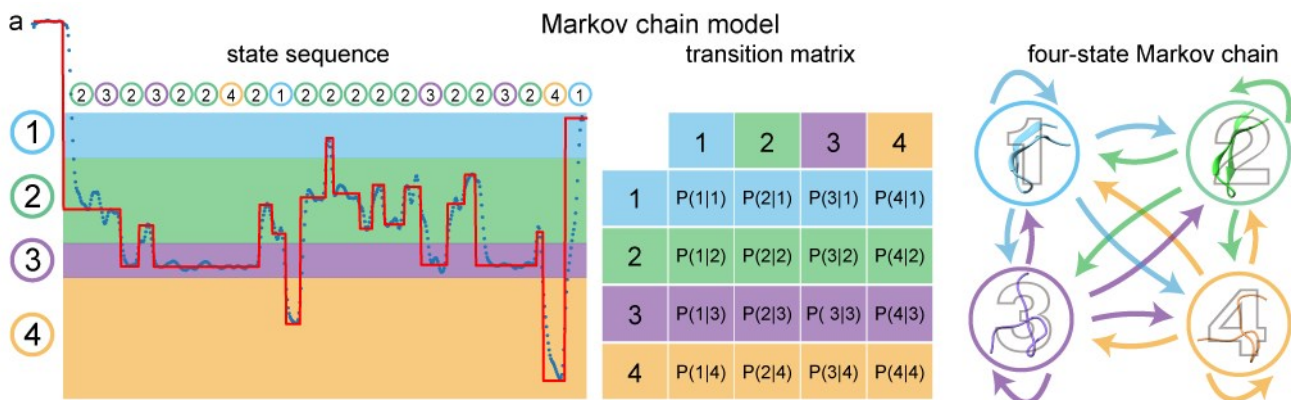


**Figure S5.** Diagram of the four-state Markov chain model that describes the state transitions.

## 1.7 Molecular dynamics simulation

The MD simulation of the  $\beta$ -hairpin peptide was performed by the AMBER16 program. The initial coordinates of the G-hairpin peptide that consists of the C-terminal residues 41-56 was taken from Protein Data Bank (PDB code: 1GB1) were constructed starting from the C-terminal residues 41 to 56 of crystal structure 1GB1 (Protein Data Bank ID), The Amber14SB force field was used for the peptide. The system was and immersed solvated with TIP3P water molecules in a truncated octahedral box with a margin of 10 Å along each dimension. The system was energy minimized by decreased force restraints to the protein heavy atoms. After that, the system was gradually heated from 0 K to 300 K over 60 ps in an NVT ensemble and equilibrated at 300 K for 50 ps. Finally, a 60 ns of unrestrained MD simulation was conducted under the NPT ensemble at 300 K and 1 atm. The SHAKE algorithm was used to constrain the covalent bonds involving hydrogen atoms. The Particle Mesh Ewald method was applied to compute the long-range electrostatic interactions. All the simulation data were analyzed and viewed depicted using the VMD software program.<sup>11,12</sup>

## 2 Results and Discussion

### 2.1 Control experiment of $\beta$ -hairpin peptide and monovalent streptavidin detection.



**Figure S6.** The raw current trace for  $\beta$ -hairpin with a SiNx nanopore. The final concentration of  $\beta$ -hairpin is 5 nM in nanopore measurement. All the data is acquired at + 150 mV in 1 M KCl, 10 mM Tris-HCL, pH 8.0.



**Figure S7.** The raw current trace for monovalent streptavidin with a  $\sim 4$ nm SiNx nanopore. The final concentration of monovalent streptavidin is 5 nM in nanopore measurement. All the data is acquired at + 150 mV in 1 M KCl, 10 mM Tris-HCL, pH 8.0. The mSA alone hardly produces any blockages by using a  $\sim 4$  nm SiNx nanopore since the size of mSA is larger than the size of the nanopore. In addition, the mSA has a large molecular weight with a less net charge which owns the isoelectric point about  $\sim 7.0$ .<sup>13</sup> Therefore, mSA is difficult to be captured by nanopore by the electric field force.

## 2.2 Raw current trace of the peptide-mSA complex detection with different voltage.

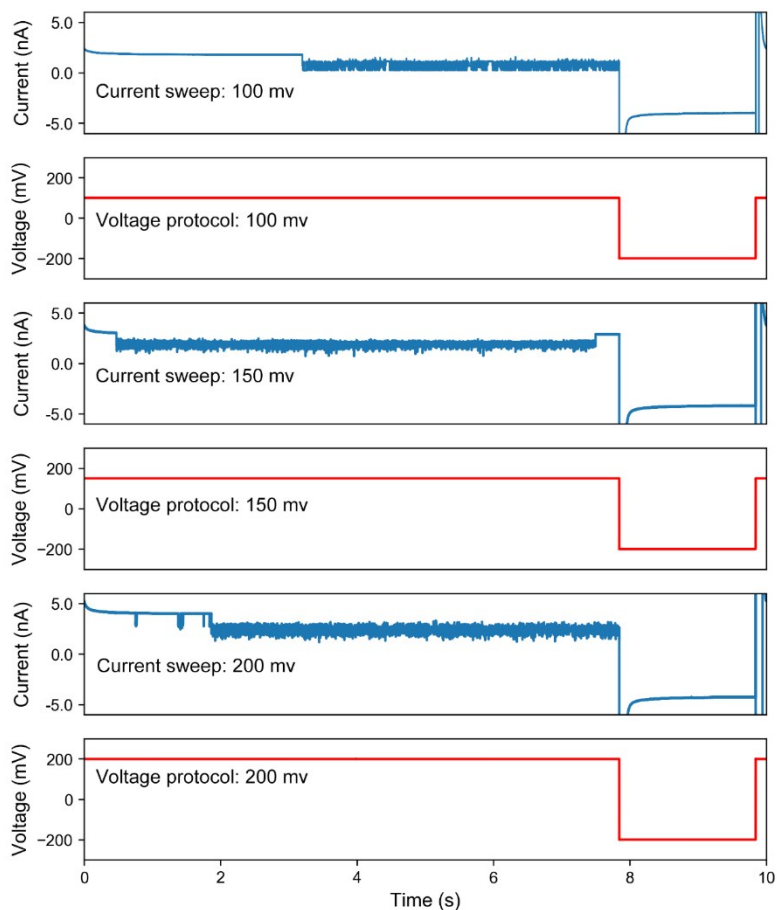


**Figure S8.** The raw current trace and data acquisition protocol with different applied voltage. The data acquisition is using the sweep mode with 7 s positive voltage to capture a peptide-mSA complex and 3 s negative voltage to release the complex.

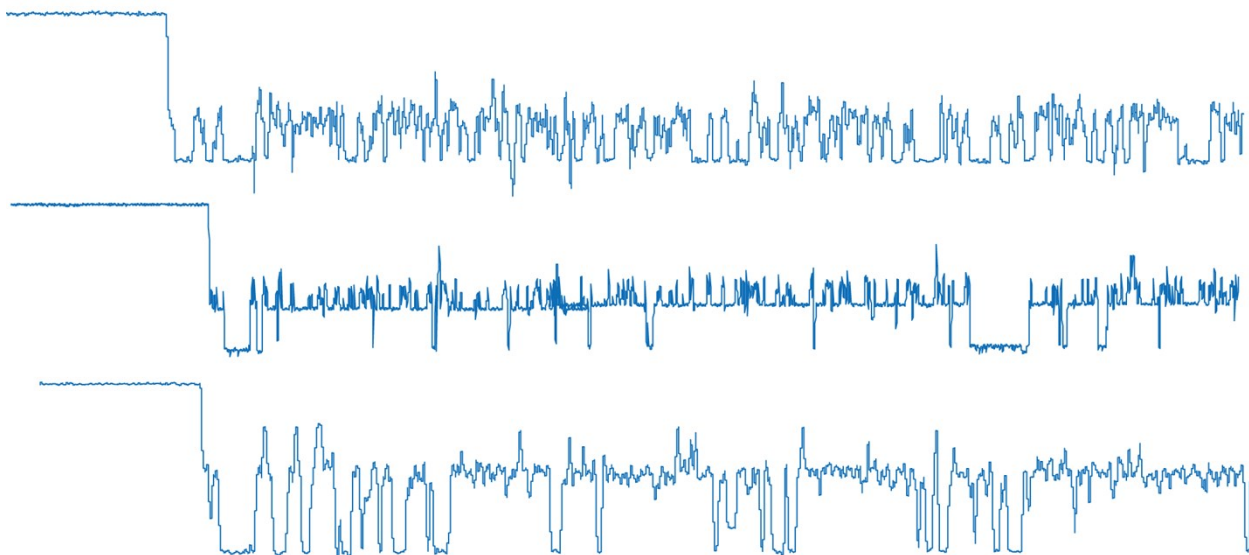


**Figure S9.** Examples of the raw current signal details. The current signal for each peptide has several different current stages.

### 2.3 The scatter plots and time probability of the example signals for the four kinds of typical current patterns.

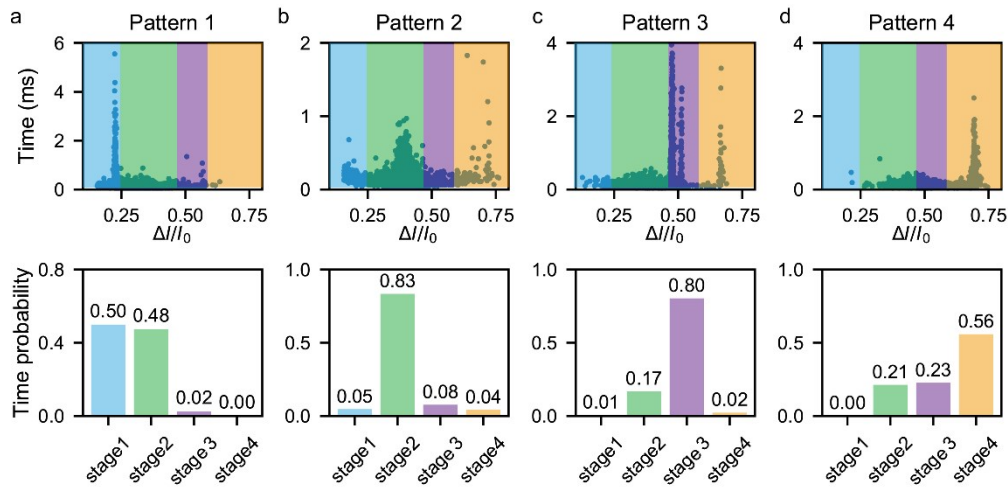


**Figure S10.** Scatter plots of the spikes and time probability of the sum durations at each stage to the entire lifetime of the typical event of pattern 1 (a), pattern 2 (b), pattern 3 (c) and pattern 4 (d) as shown in Figure 2b-e.

### 2.4 The confined effects on the time probability of single $\beta$ -hairpin for each current stage.

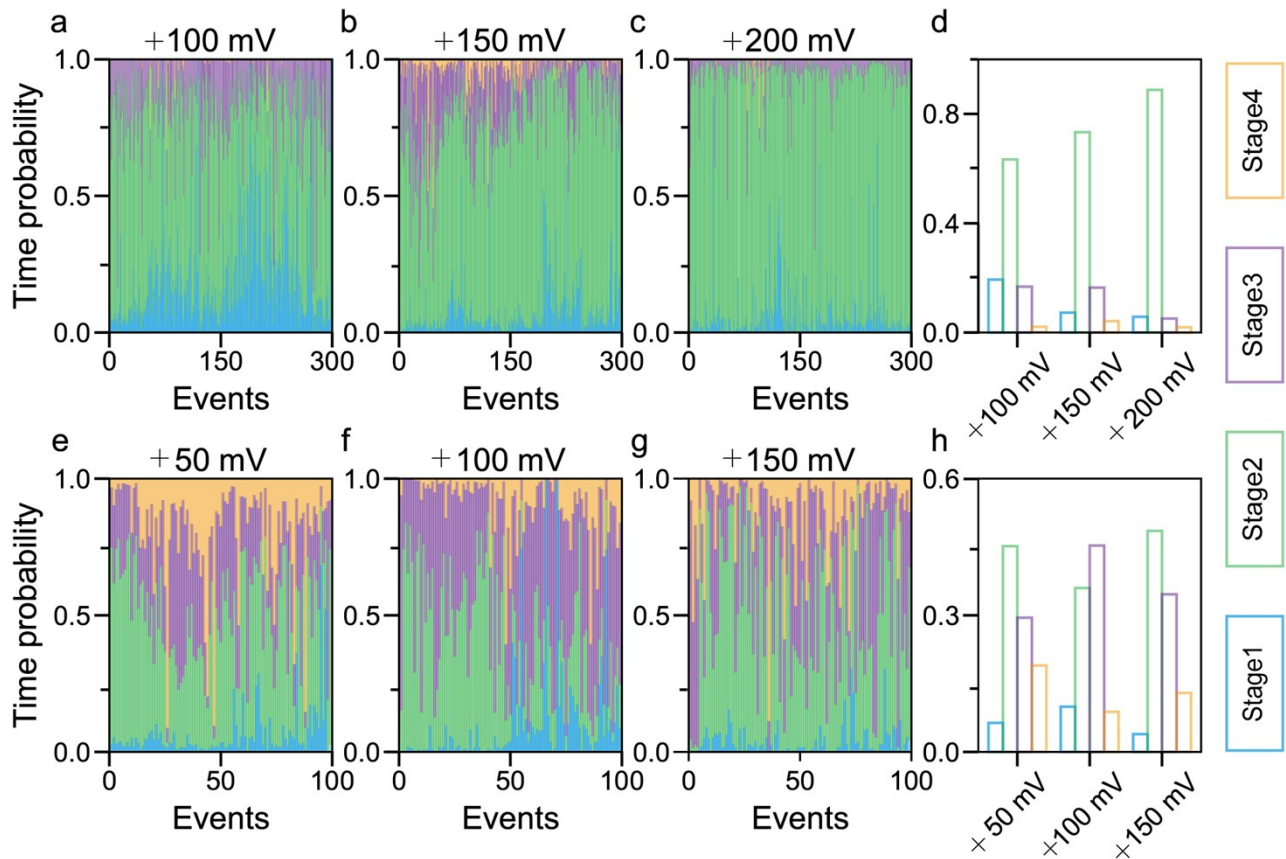


**Figure S11.** The confined effects on the time probability of single  $\beta$ -hairpin for each current stage. The stacked bar charts for the time probability of each event under (a) +100 mV, (b) +150 mV and (c) +200 mV using  $d \sim 4$  nm nanopore. (d) the voltage-dependent average time probability from all the events of each current stage using  $d \sim 4$  nm nanopore. The stacked bar charts for the time probability of each event under (e) +50 mV, (f) +100 mV and (g) +150 mV using  $d \sim 5$  nm nanopore. (h) The voltage-dependent average time probability from all the events of each current stage using  $d \sim 5$  nm nanopore. Stage 1 to 4 are colored by blue, green, purple and orange.

2.5 Sequence .dependent conformational dynamics of single  $\beta$ -hairpin

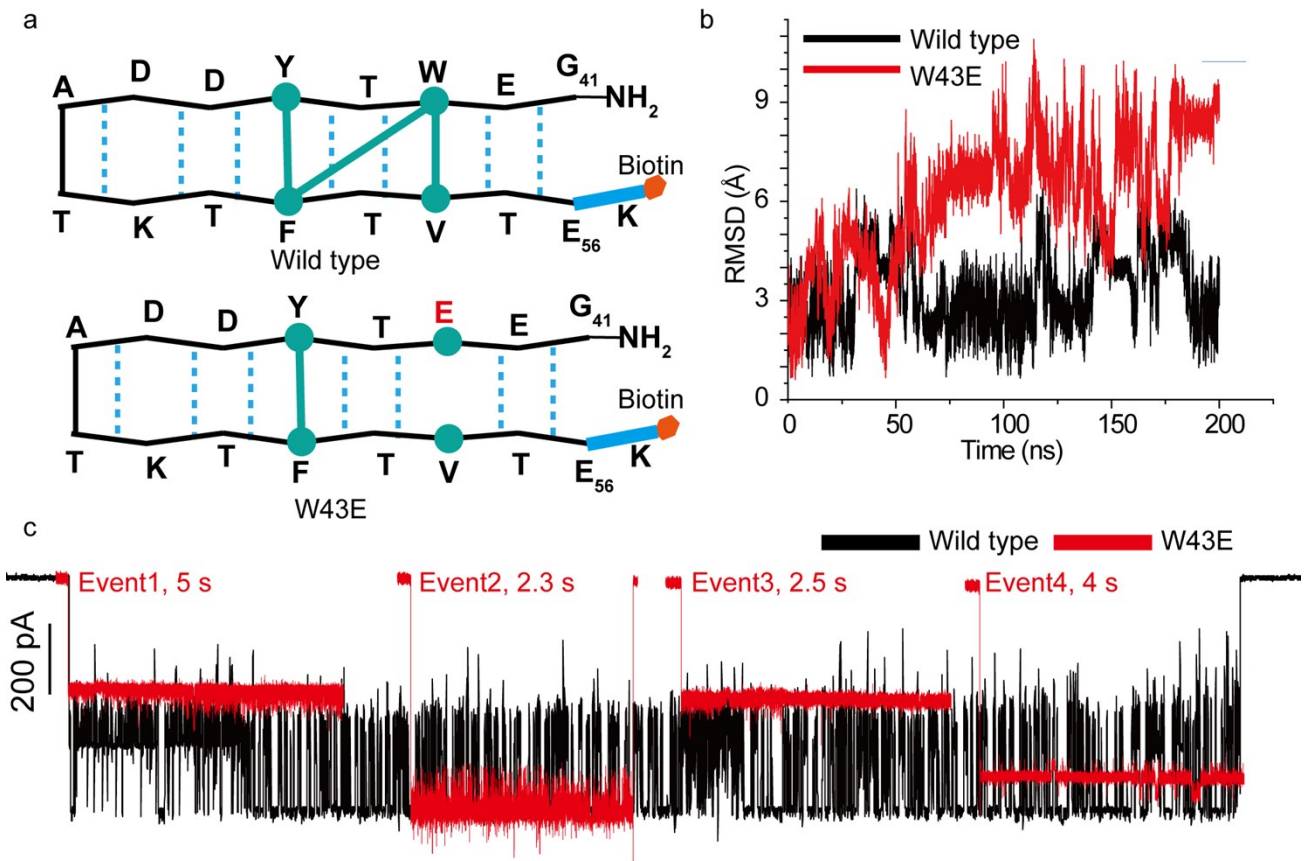


**Figure S12.** (a) The amino acid sequence of wild type and mutant W43E  $\beta$ -hairpin peptide. (b) The RMSD of peptide backbone atoms to energy minimized structure as a function of simulation time for wild type and mutant W43E  $\beta$ -hairpin structure conforming to the dynamic folding state within 200 ns. (c) The characteristic current signal of wild type and mutant W43E  $\beta$ -hairpin peptide.

2.6 Current histogram of single peptide events with  $d \sim 4$  nm nanopore under +100 mV.

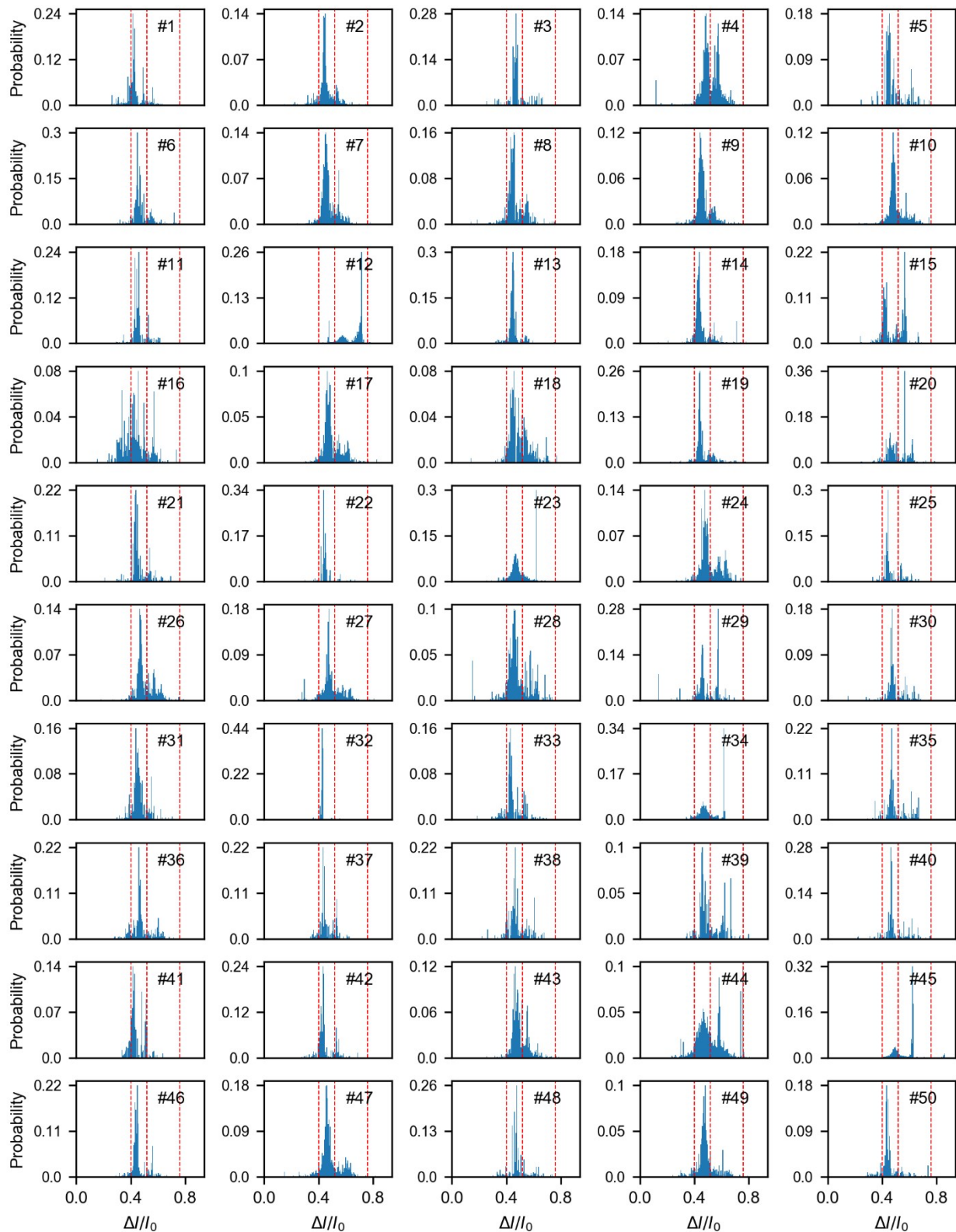


**Figure S13.** The current histogram of single peptide events from event 1 to 50. Each peptide produces the characteristic current distributions which could be divided into four stages by the dashed line with  $\Delta/I_0 = 0.4, 0.52$  and  $0.76$  from left to right assigned as stage 1, stage 2, stage 3 and stage 4, respectively. All the data is acquired at + 100 mV in 1 M KCl, 10 mM Tris-HCL, pH 8.0 with a  $d \sim 4$  nm nanopore.

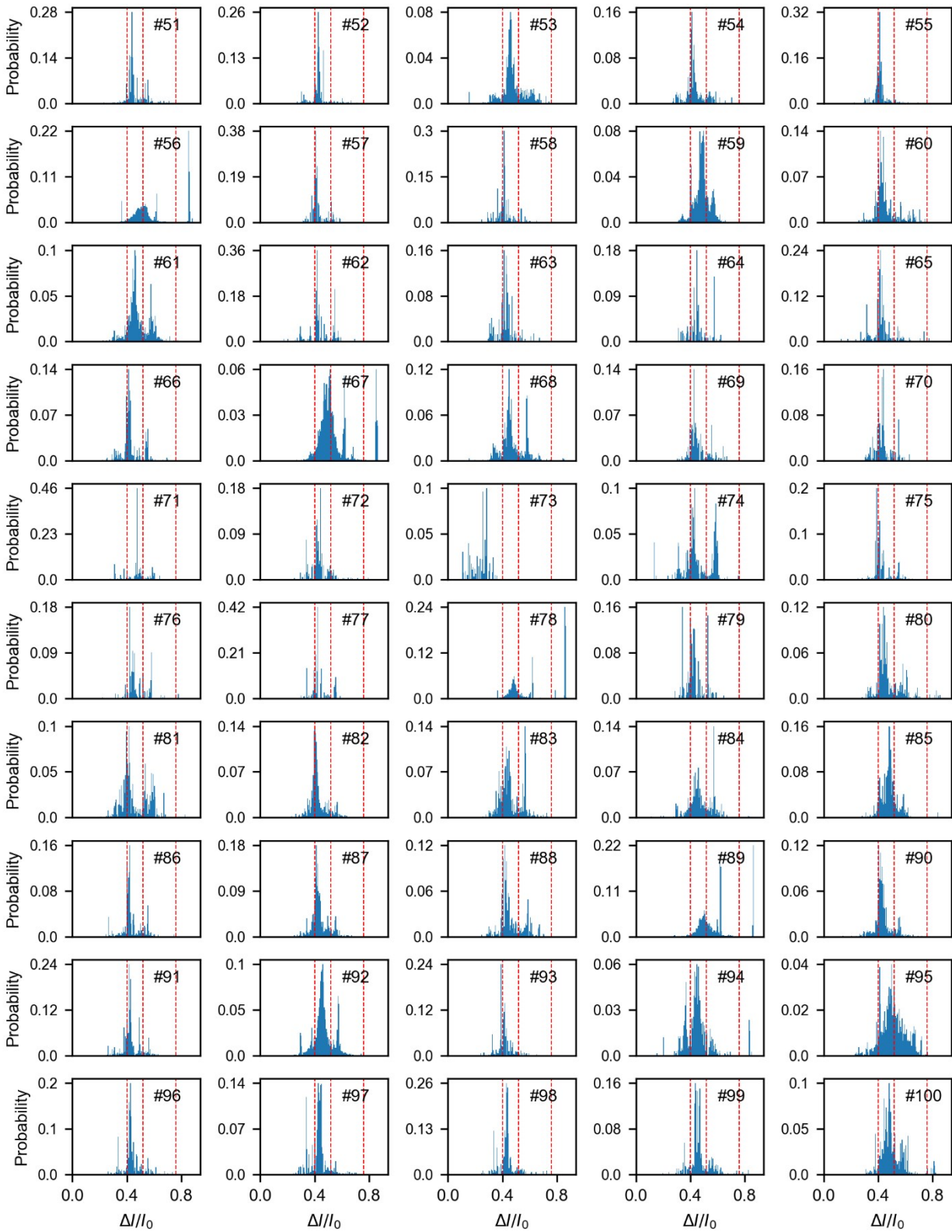


**Figure S14. The current histogram of single peptide events from event 51 to 100.** Each peptide produces the characteristic current distributions which could be divided into four stages by the dashed line with  $\Delta I/I_0 = 0.4, 0.52$  and  $0.76$  from left to right assigned as stage 1, stage 2, stage 3 and stage 4, respectively. All the data is acquired at  $+100$  mV in  $1$  M KCl,  $10$  mM Tris-HCl, pH  $8.0$  with a  $d \sim 4$  nm nanopore.

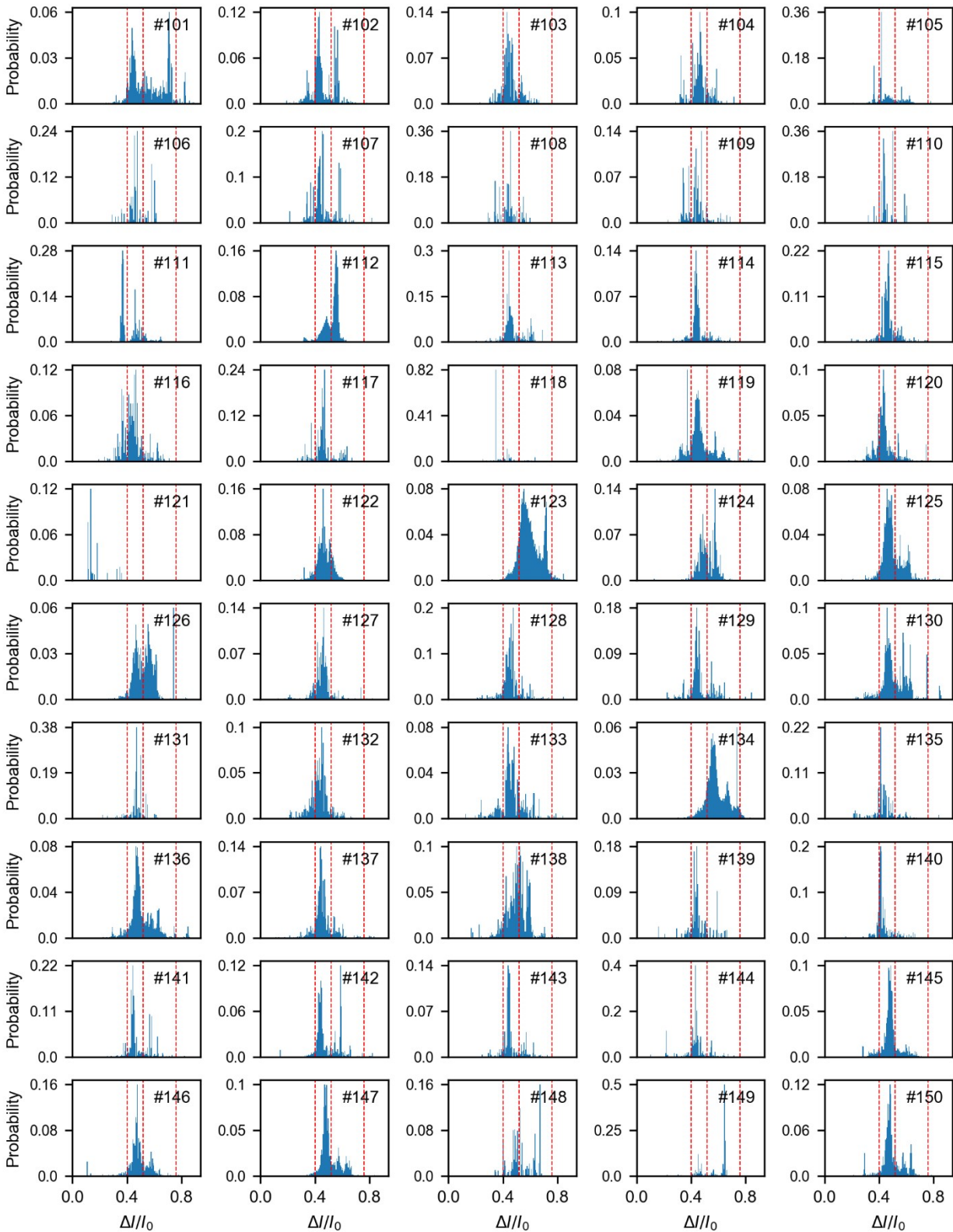


**Figure S15. The current histogram of single peptide events from event 101 to 150.** Each peptide produces the characteristic current distributions which could be divided into four stages by the dashed line with  $\Delta I/I_0 = 0.4, 0.52$  and  $0.76$  from left to right assigned as stage 1, stage 2, stage 3 and stage 4, respectively. All the data is acquired at +100 mV in 1 M KCl, 10 mM Tris-HCl, pH 8.0 with a  $d \sim 4$  nm nanopore.

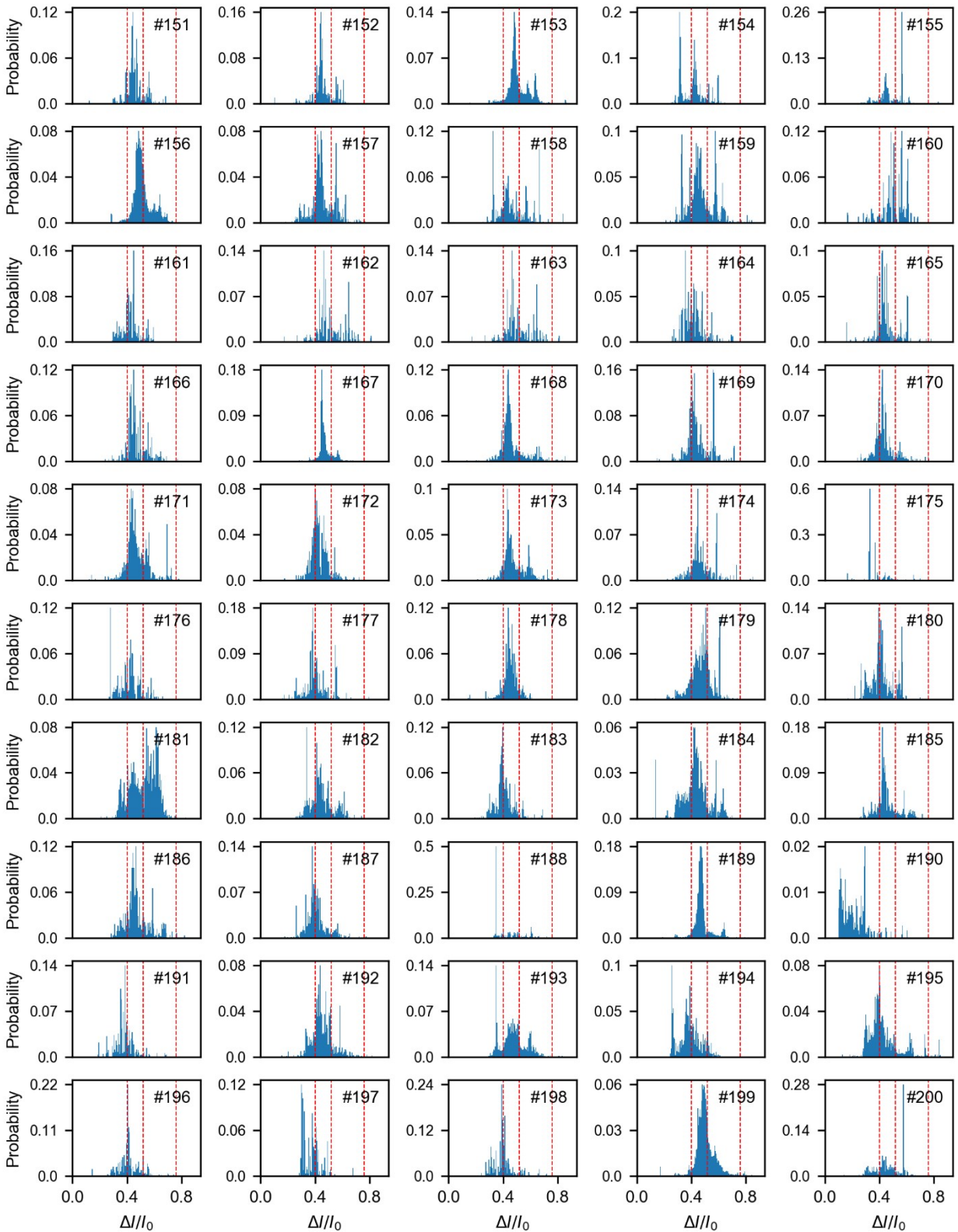


**Figure S16. The current histogram of single peptide events from event 151 to 200.** Each peptide produces the characteristic current distributions which could be divided into four stages by the dashed line with  $\Delta I/I_0 = 0.4, 0.52$  and  $0.76$  from left to right assigned as stage 1, stage 2, stage 3 and stage 4, respectively. All the data is acquired at +100 mV in 1 M KCl, 10 mM Tris-HCl, pH 8.0 with a  $d \sim 4$  nm nanopore.

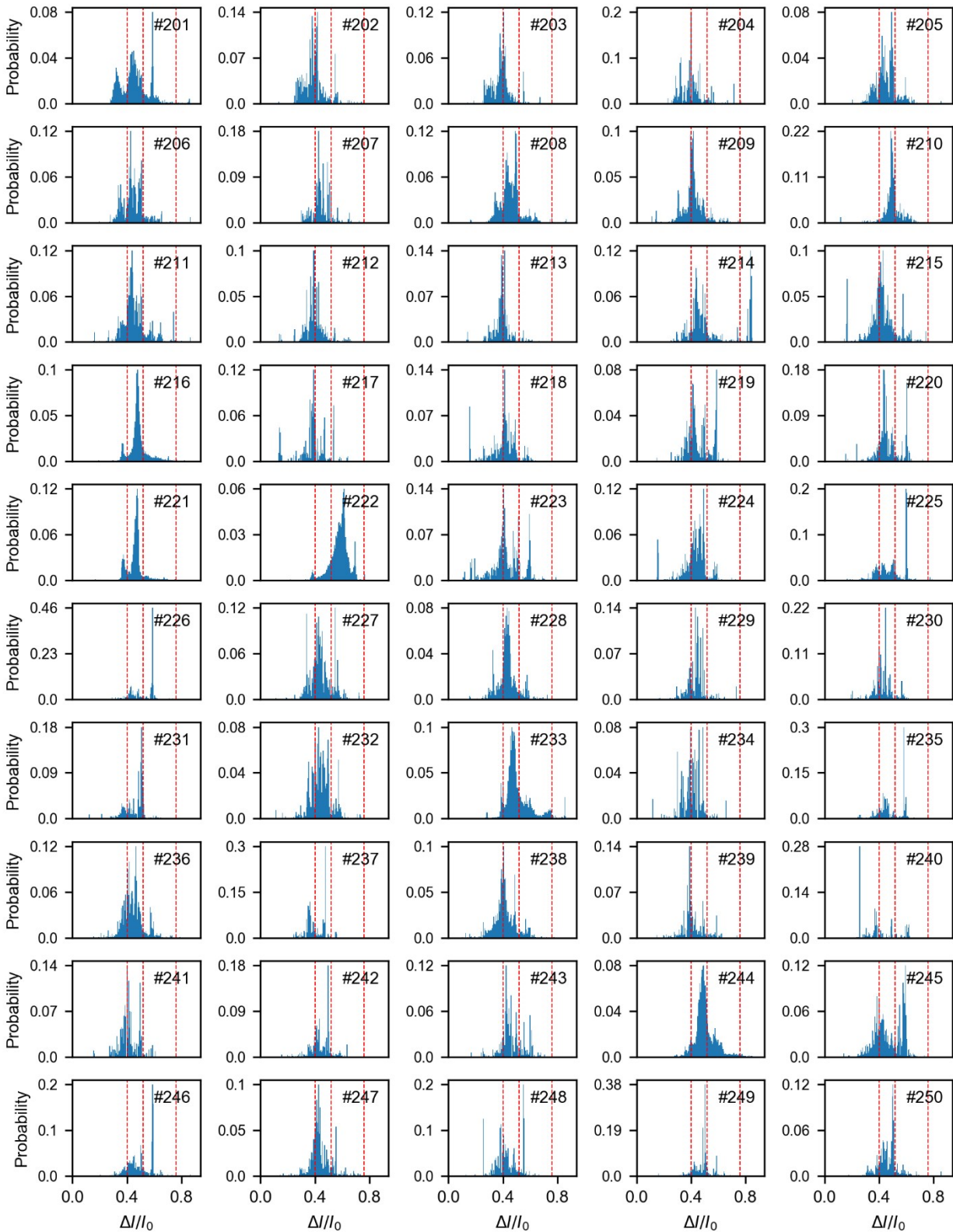


**Figure S17. The current histogram of single peptide events from event 201 to 250.** Each peptide produces the characteristic current distributions which could be divided into four stages by the dashed line with  $\Delta I/I_0 = 0.4, 0.52$  and  $0.76$  from left to right assigned as stage 1, stage 2, stage 3 and stage 4, respectively. All the data is acquired at +100 mV in 1 M KCl, 10 mM Tris-HCl, pH 8.0 with a  $d \sim 4$  nm nanopore.

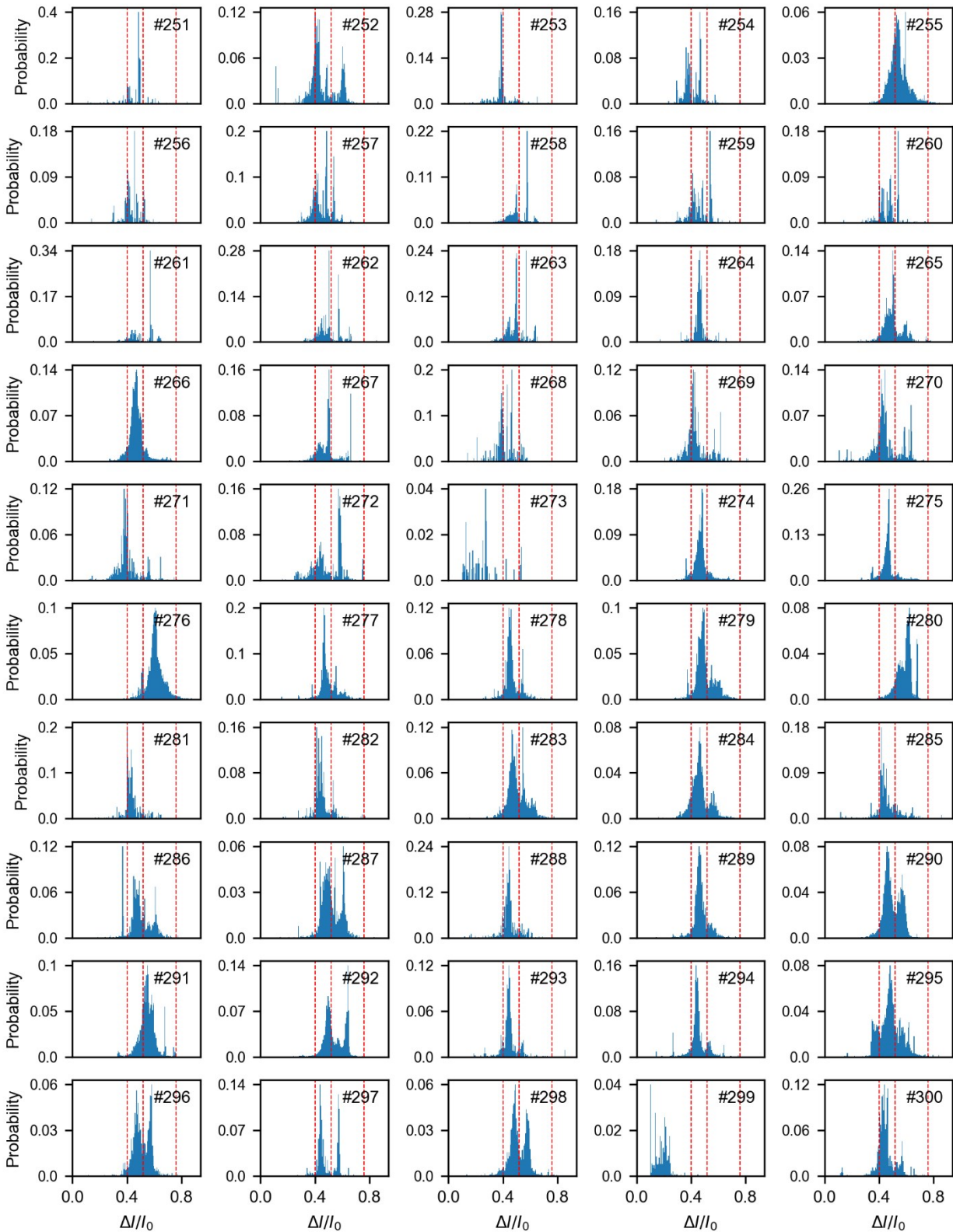


**Figure S18. The current histogram of single peptide events from event 251 to 300.** Each peptide produces the characteristic current distributions which could be divided into four stages by the dashed line with  $\Delta I/I_0 = 0.4, 0.52$  and  $0.76$  from left to right assigned as stage 1, stage 2, stage 3 and stage 4, respectively. All the data is acquired at +100 mV in 1 M KCl, 10 mM Tris-HCl, pH 8.0 with a  $d \sim 4$  nm nanopore.

2.7 Current histogram of single peptide events with  $d \sim 4$  nm nanopore under +150 mV.

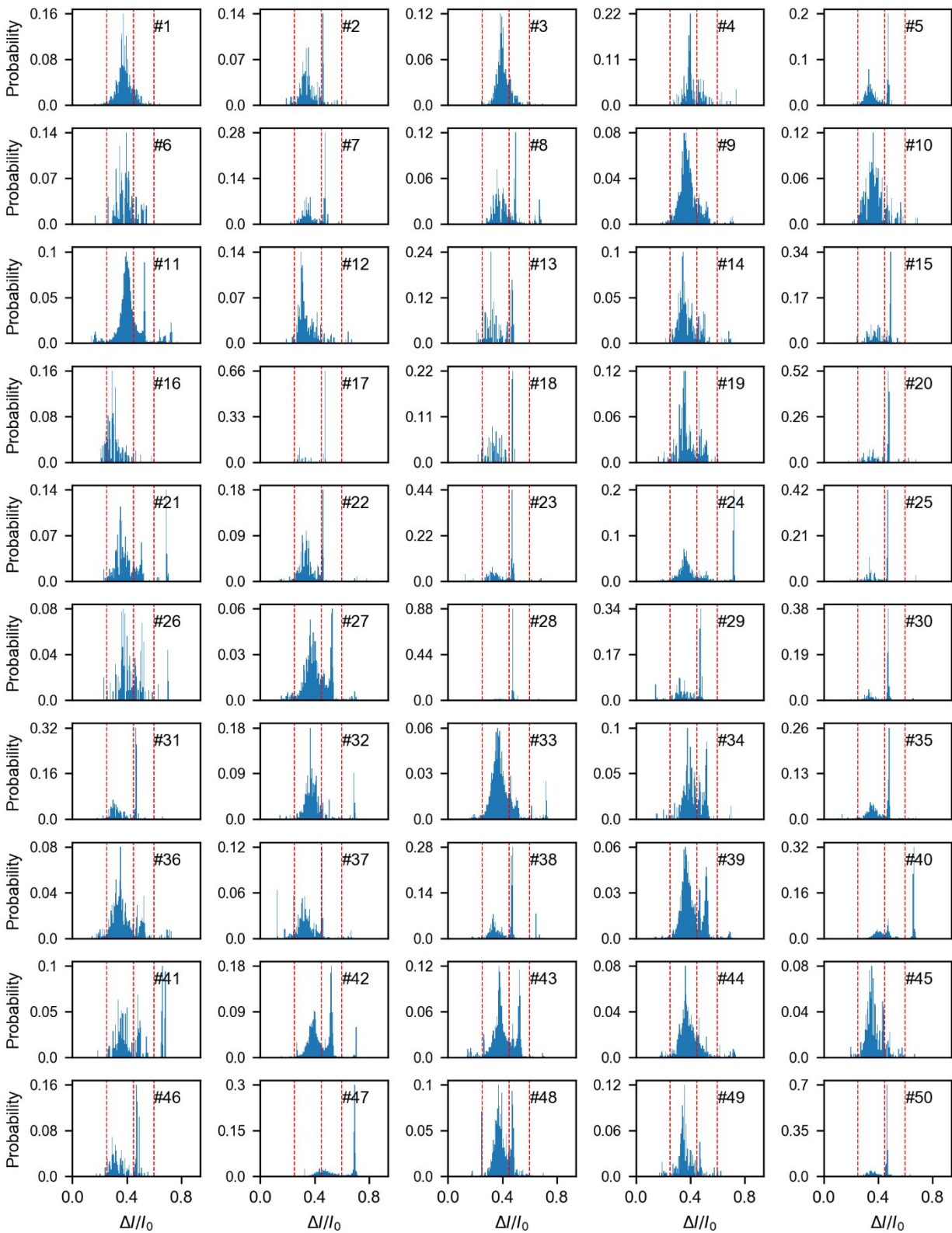


**Figure S19.** The current histogram of single peptide events from event 1 to 50. Each peptide produces the characteristic current distributions which could be divided into four stages by the dashed line with  $\Delta I/I_0 = 0.24, 0.46$  and  $0.58$  from left to right assigned as stage 1, stage 2, stage 3 and stage 4, respectively. All the data is acquired at +150 mV in 1 M KCl, 10 mM Tris-HCl, pH 8.0 with a  $d \sim 4$  nm nanopore.

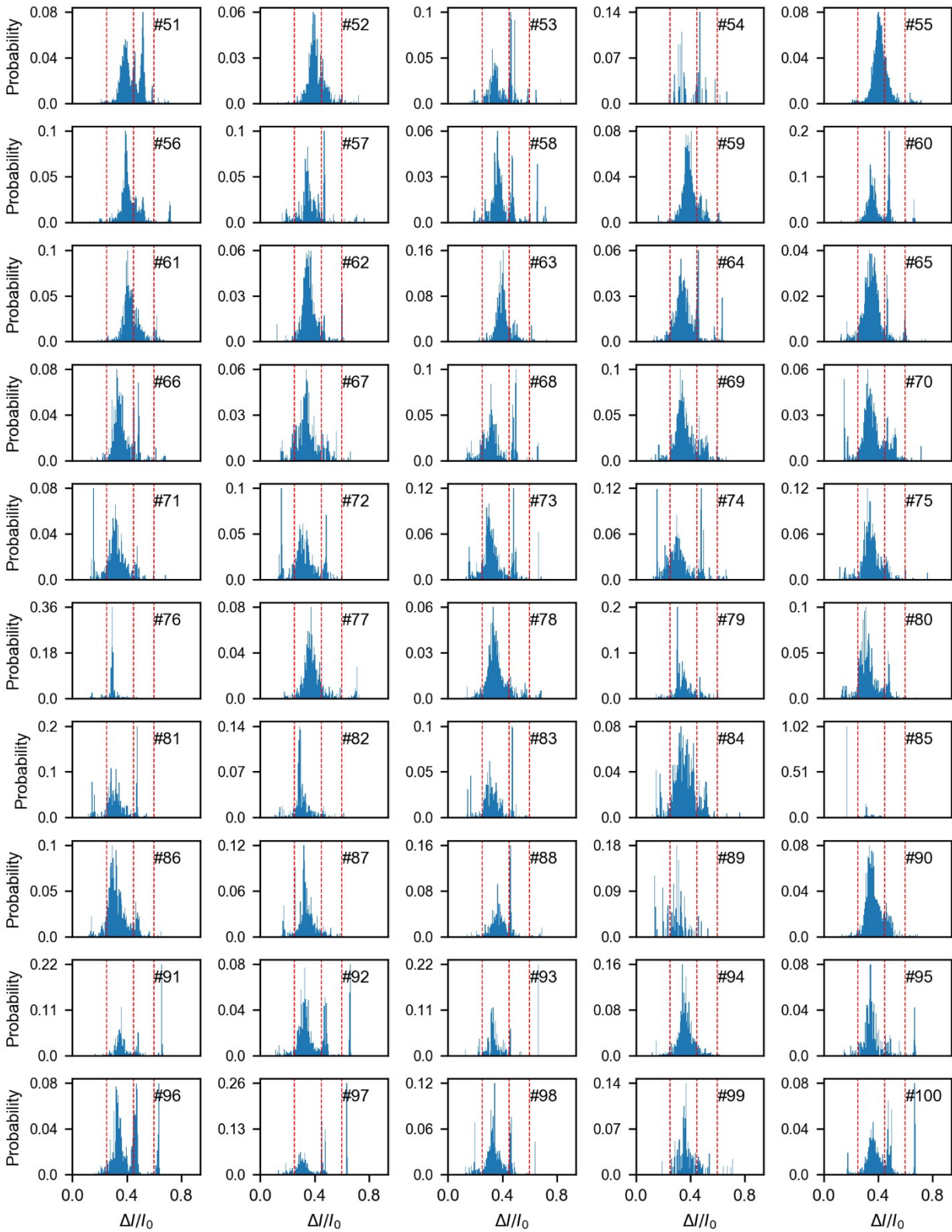


**Figure S20. The current histogram of single peptide events from event 51 to 100.** Each peptide produces the characteristic current distributions which could be divided into four stages by the dashed line with  $\Delta I/I_0 = 0.24, 0.46$  and  $0.58$  from left to right assigned as stage 1, stage 2, stage 3 and stage 4, respectively. All the data is acquired at  $+150$  mV in  $1$  M KCl,  $10$  mM Tris-HCl, pH 8.0 with a  $d \sim 4$  nm nanopore.

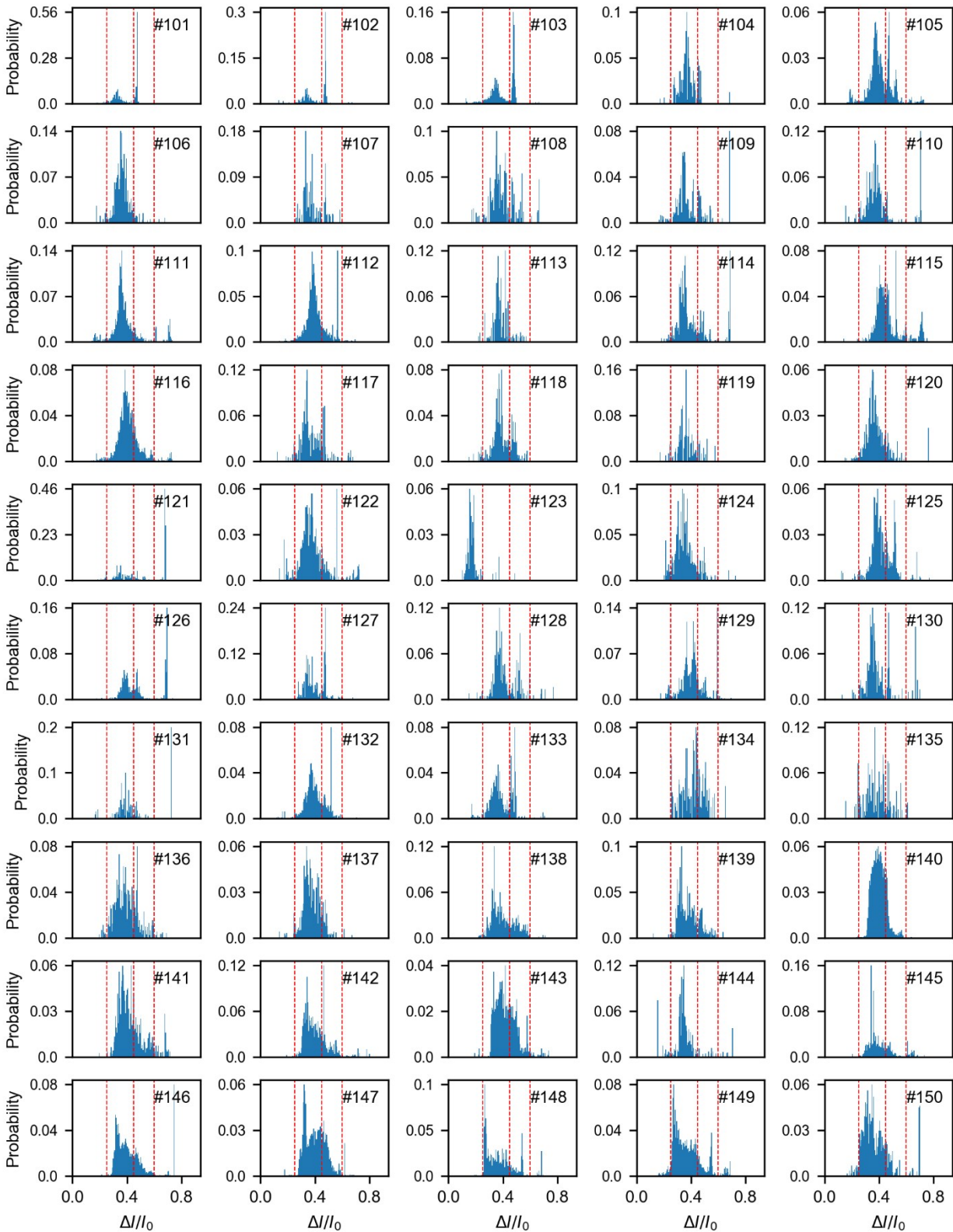


**Figure S21. The current histogram of single peptide events from event 101 to 150.** Each peptide produces the characteristic current distributions which could be divided into four stages by the dashed line with  $\Delta I/I_0 = 0.24, 0.46$  and  $0.58$  from left to right assigned as stage 1, stage 2, stage 3 and stage 4, respectively. All the data is acquired at  $+150$  mV in  $1$  M KCl,  $10$  mM Tris-HCL, pH  $8.0$  with a  $d \sim 4$  nm nanopore.

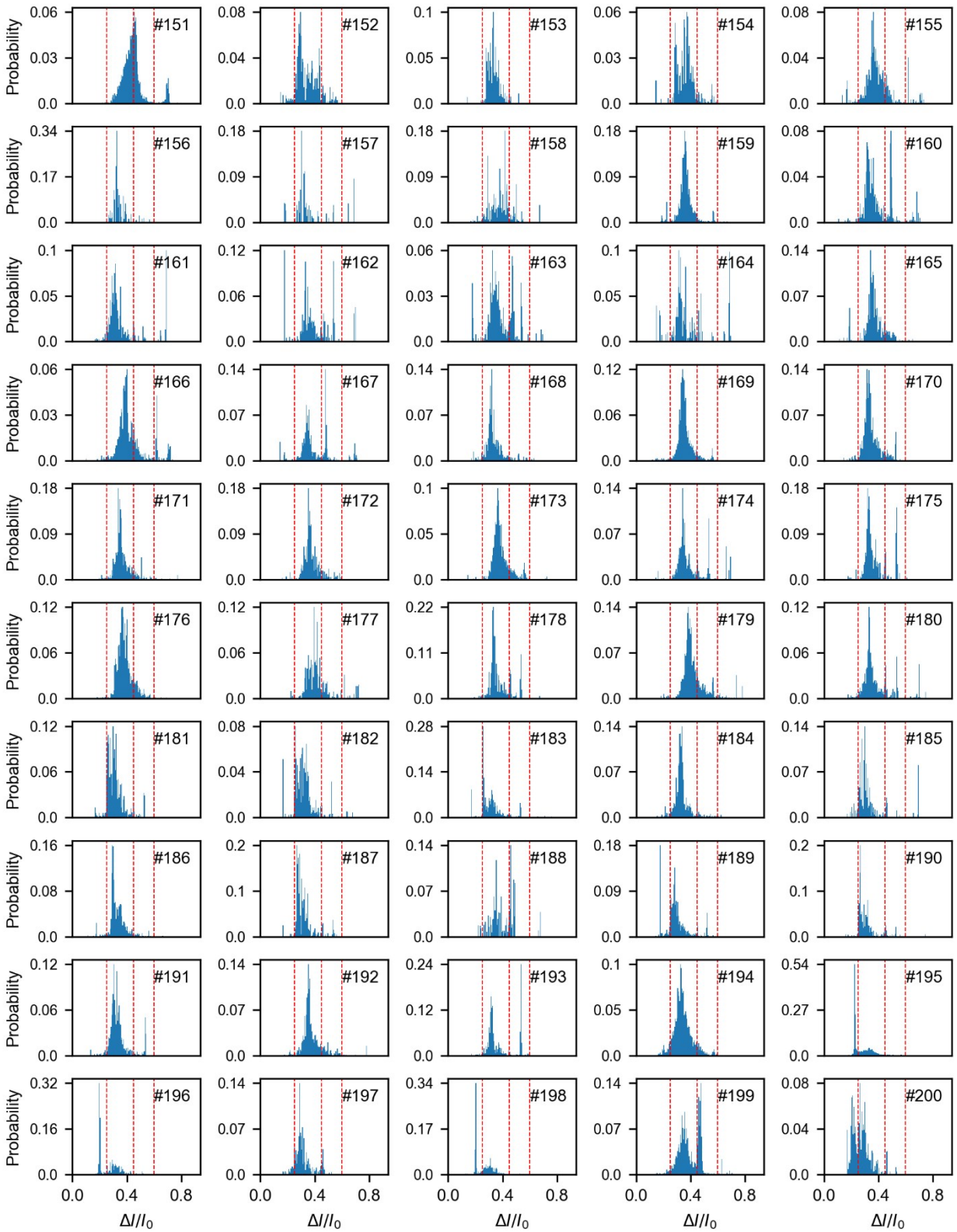


**Figure S22. The current histogram of single peptide events from event 151 to 200.** Each peptide produces the characteristic current distributions which could be divided into four stages by the dashed line with  $\Delta I/I_0 = 0.24, 0.46$  and  $0.58$  from left to right assigned as stage 1, stage 2, stage 3 and stage 4, respectively. All the data is acquired at  $+150$  mV in  $1$  M KCl,  $10$  mM Tris-HCl, pH 8.0 with a  $d \sim 4$  nm nanopore.

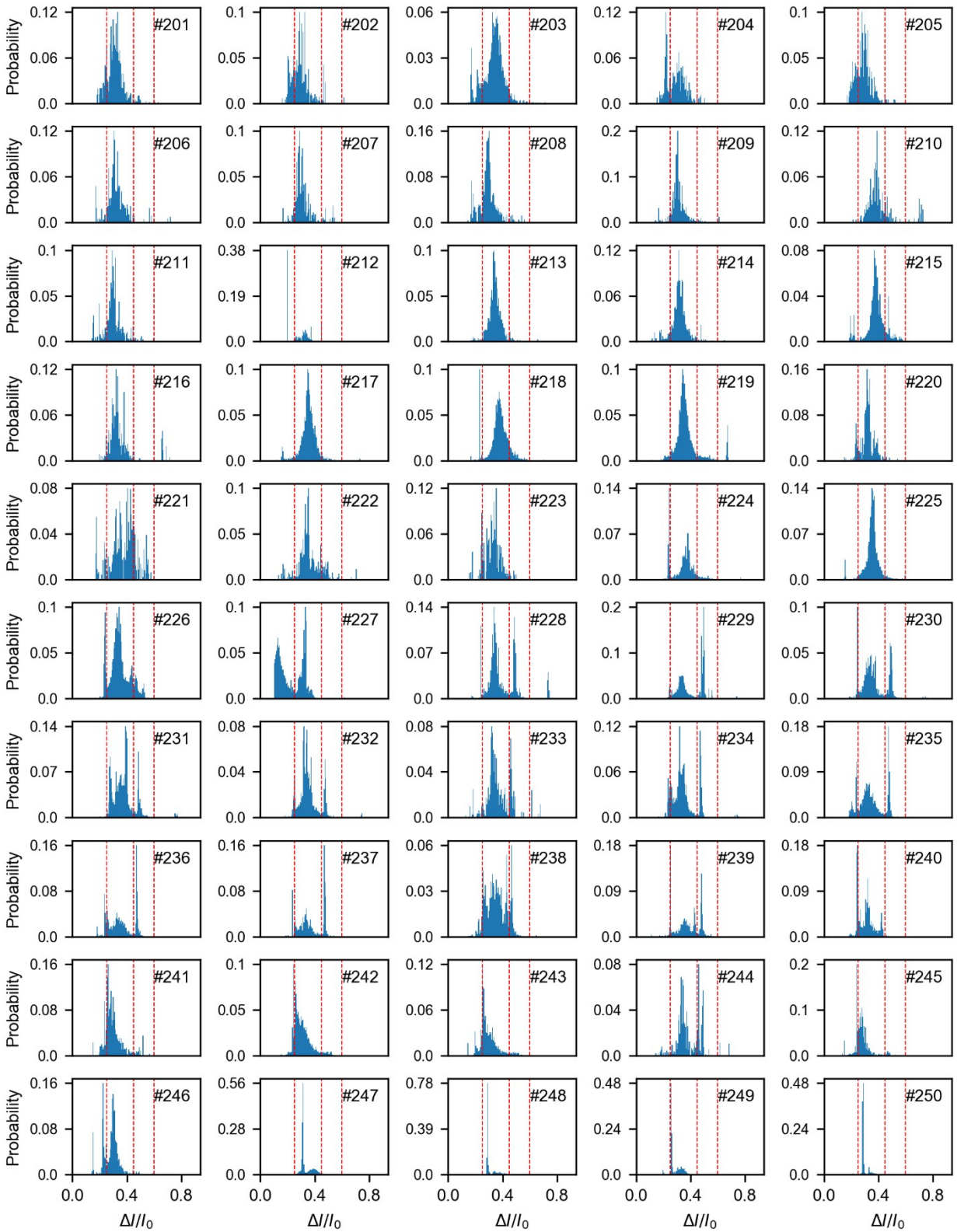


**Figure S23. The current histogram of single peptide events from event 201 to 250.** Each peptide produces the characteristic current distributions which could be divided into four stages by the dashed line with  $\Delta I/I_0 = 0.24, 0.46$  and  $0.58$  from left to right assigned as stage 1, stage 2, stage 3 and stage 4, respectively. All the data is acquired at  $+150$  mV in  $1$  M KCl,  $10$  mM Tris-HCl, pH 8.0 with a  $d \sim 4$  nm nanopore.

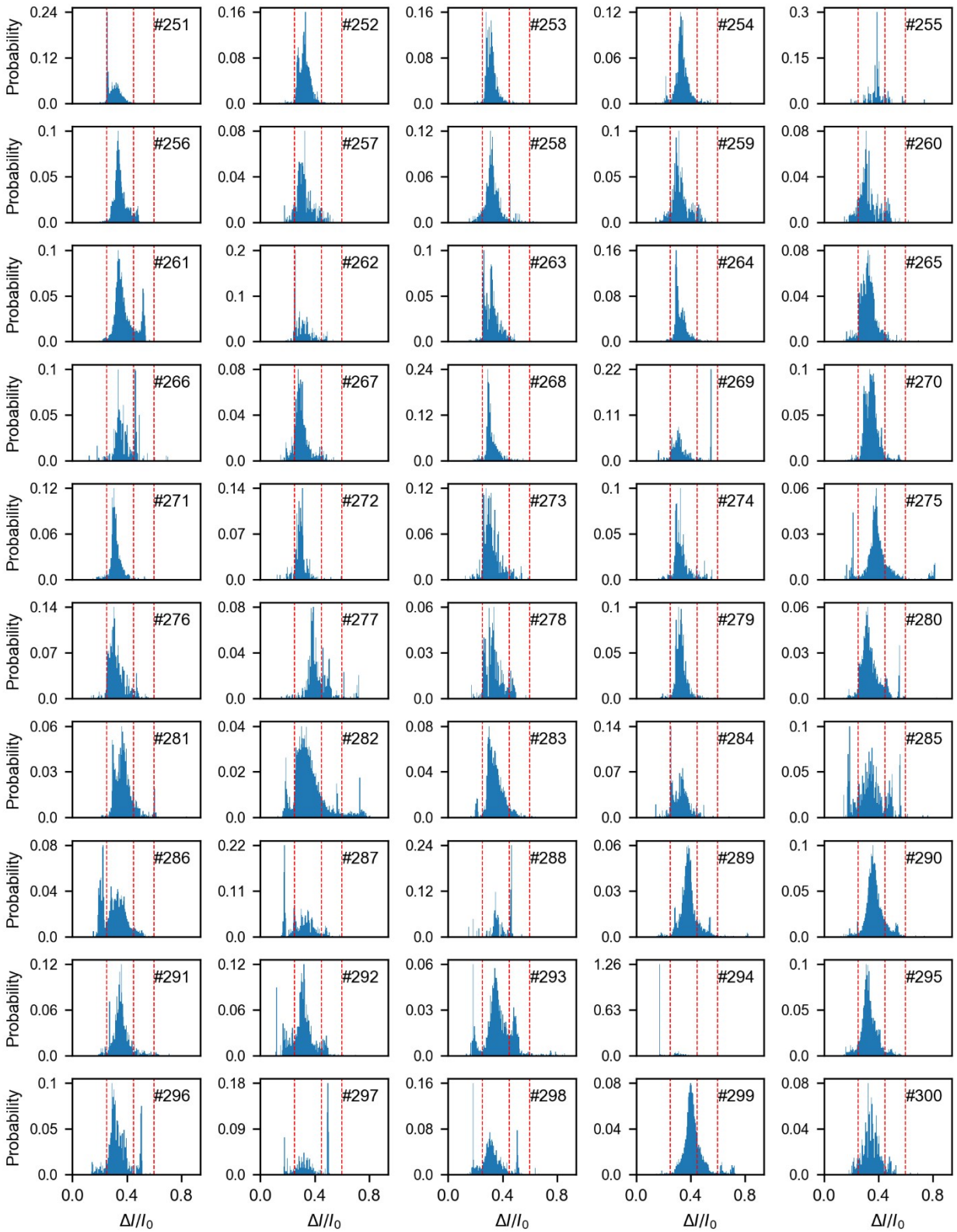


**Figure S24. The current histogram of single peptide events from event 251 to 300.** Each peptide produces the characteristic current distributions which could be divided into four stages by the dashed line with  $\Delta I/I_0 = 0.24, 0.46$  and  $0.58$  from left to right assigned as stage 1, stage 2, stage 3 and stage 4, respectively. All the data is acquired at  $+150$  mV in  $1$  M KCl,  $10$  mM Tris-HCL, pH  $8.0$  with a  $d \sim 4$  nm nanopore.

## 2.8 Current histogram of single peptide events with $d \sim 4$ nm nanopore under +200 mV.

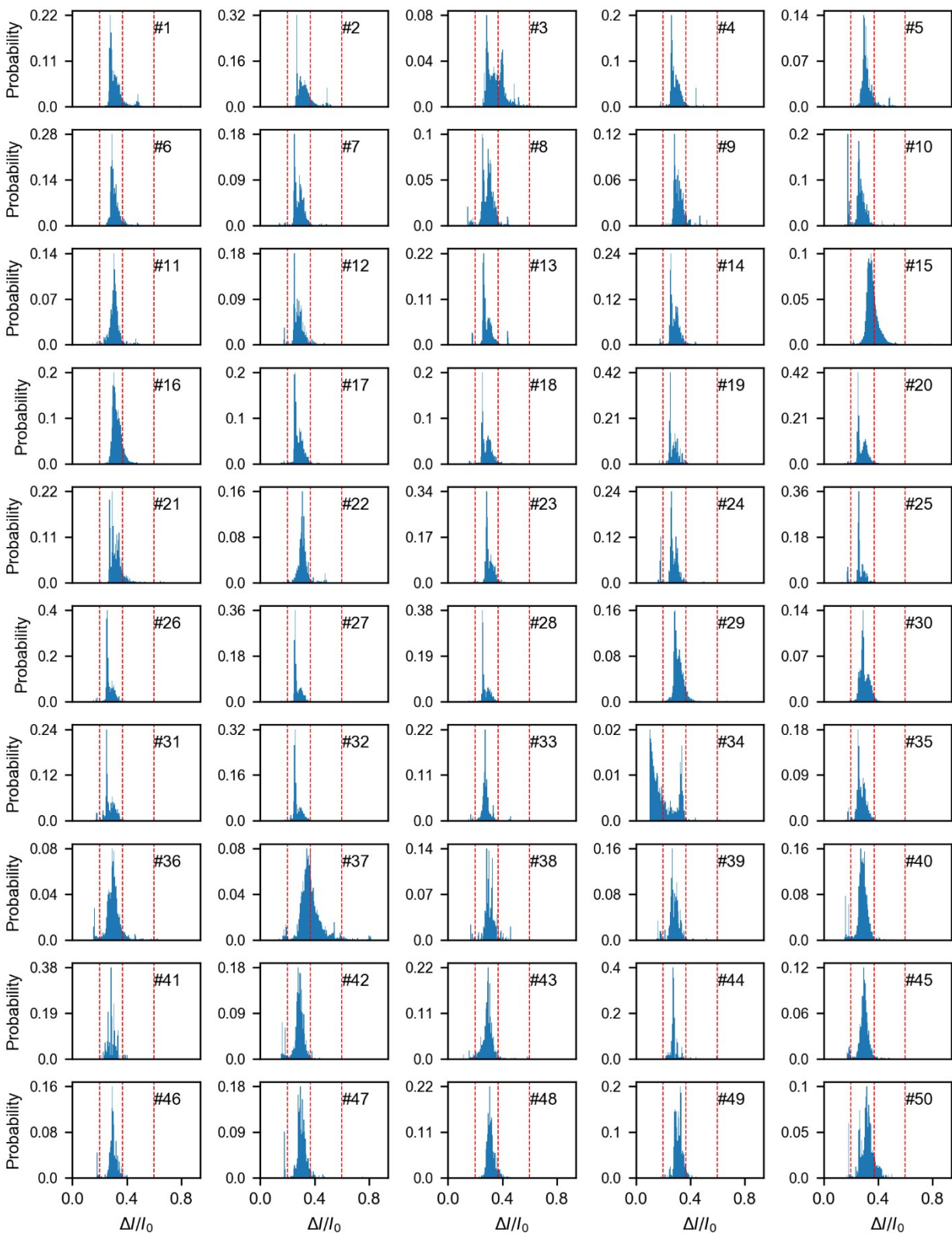


**Figure S25. The current histogram of single peptide events from event 1 to 50.** Each peptide produces the characteristic current distributions which could be divided into four stages by the dashed line with  $\Delta I/I_0 = 0.2, 0.37$  and  $0.6$  from left to right assigned as stage 1, stage 2, stage 3 and stage 4, respectively. All the data is acquired at + 200 mV in 1 M KCl, 10 mM Tris-HCL, pH 8.0 with a  $d \sim 4$  nm nanopore.

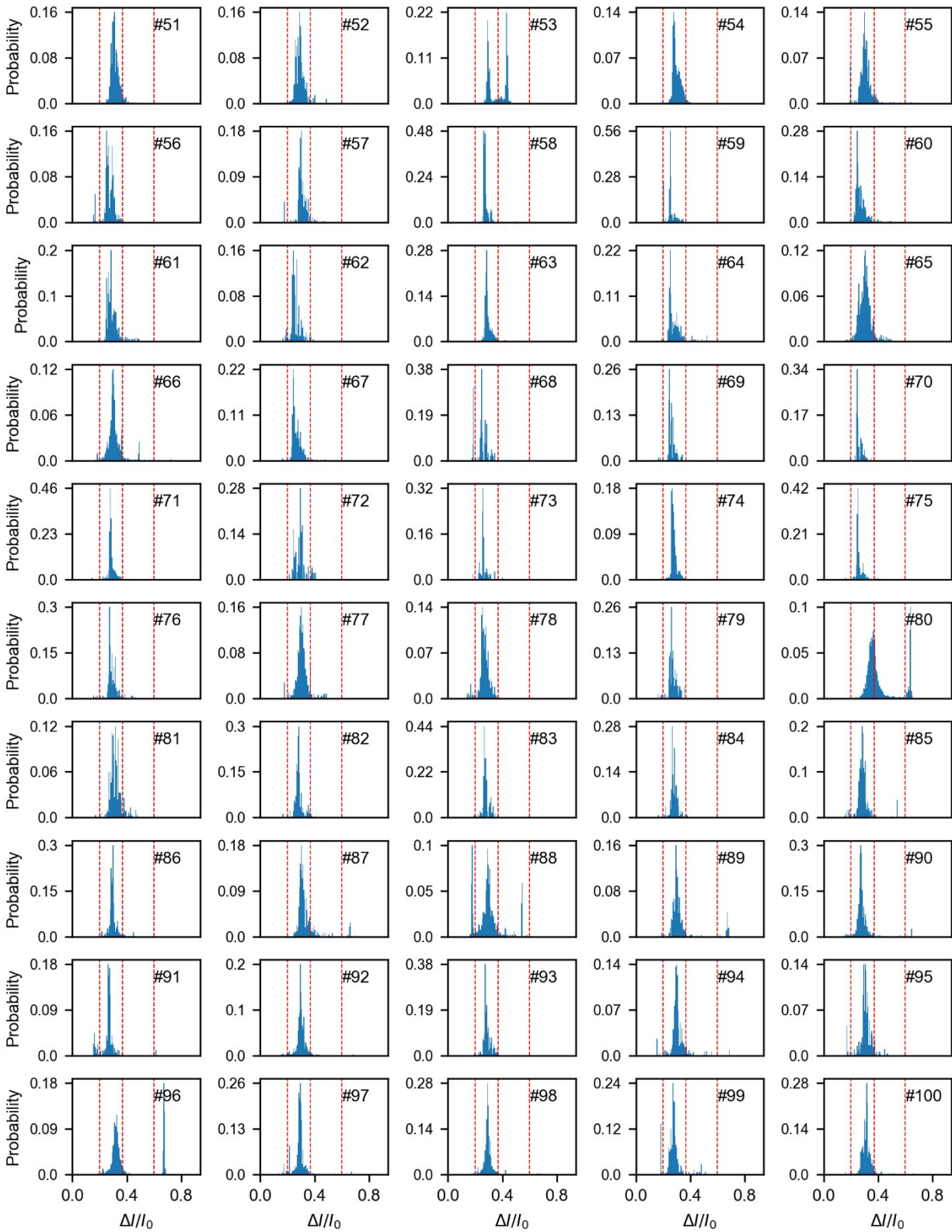


**Figure S26. The current histogram of single peptide events from event 51 to 100.** Each peptide produces the characteristic current distributions which could be divided into four stages by the dashed line with  $\Delta I/I_0 = 0.2, 0.37$  and  $0.6$  from left to right assigned as stage 1, stage 2, stage 3 and stage 4, respectively. All the data is acquired at +200 mV in 1 M KCl, 10 mM Tris-HCl, pH 8.0 with a  $d \sim 4$  nm nanopore.

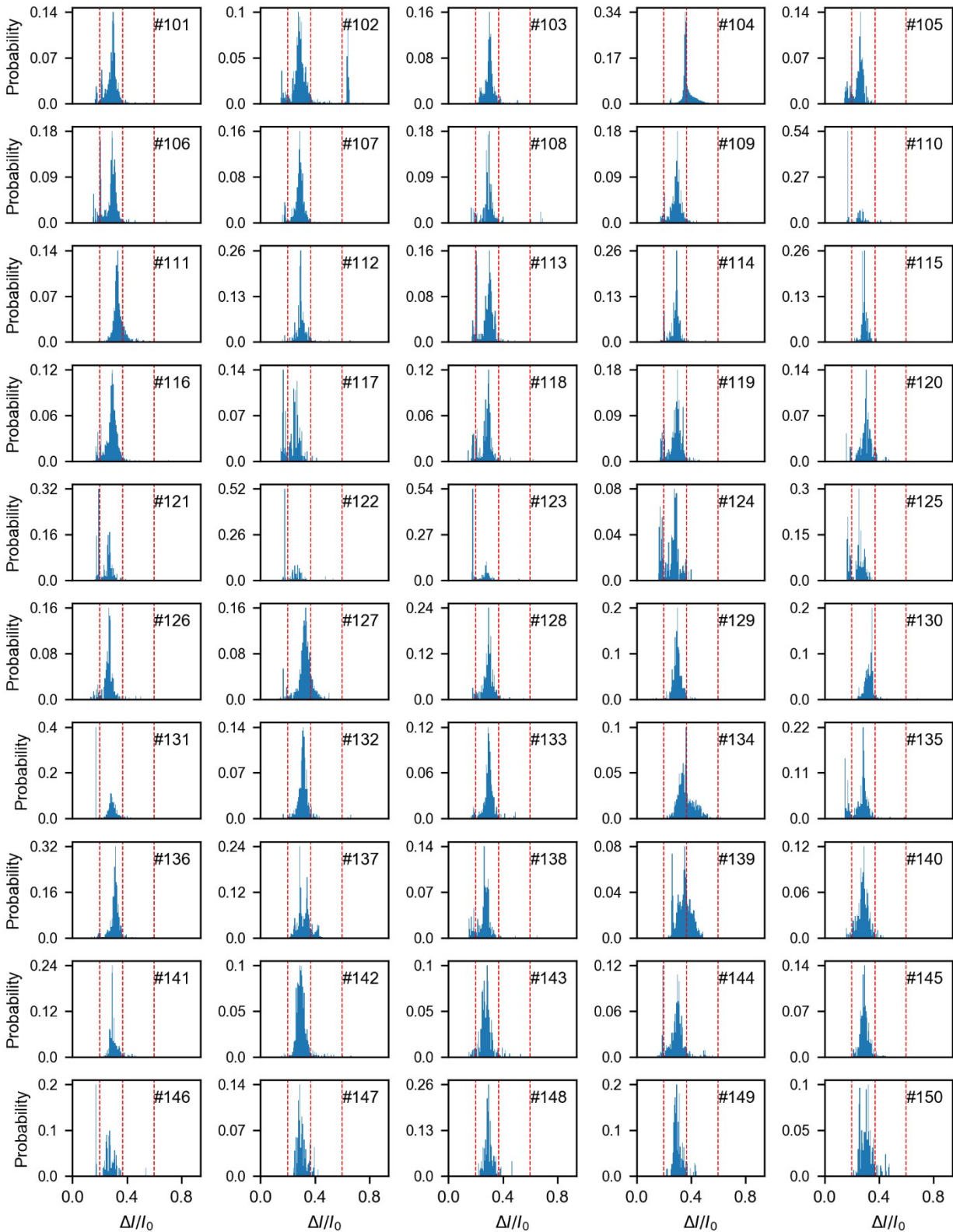


**Figure S27. The current histogram of single peptide events from event 101 to 150.** Each peptide produces the characteristic current distributions which could be divided into four stages by the dashed line with  $\Delta I/I_0 = 0.2, 0.37$  and  $0.6$  from left to right assigned as stage 1, stage 2, stage 3 and stage 4, respectively. All the data is acquired at  $+200$  mV in 1 M KCl, 10 mM Tris-HCL, pH 8.0 with a  $d \sim 4$  nm nanopore.

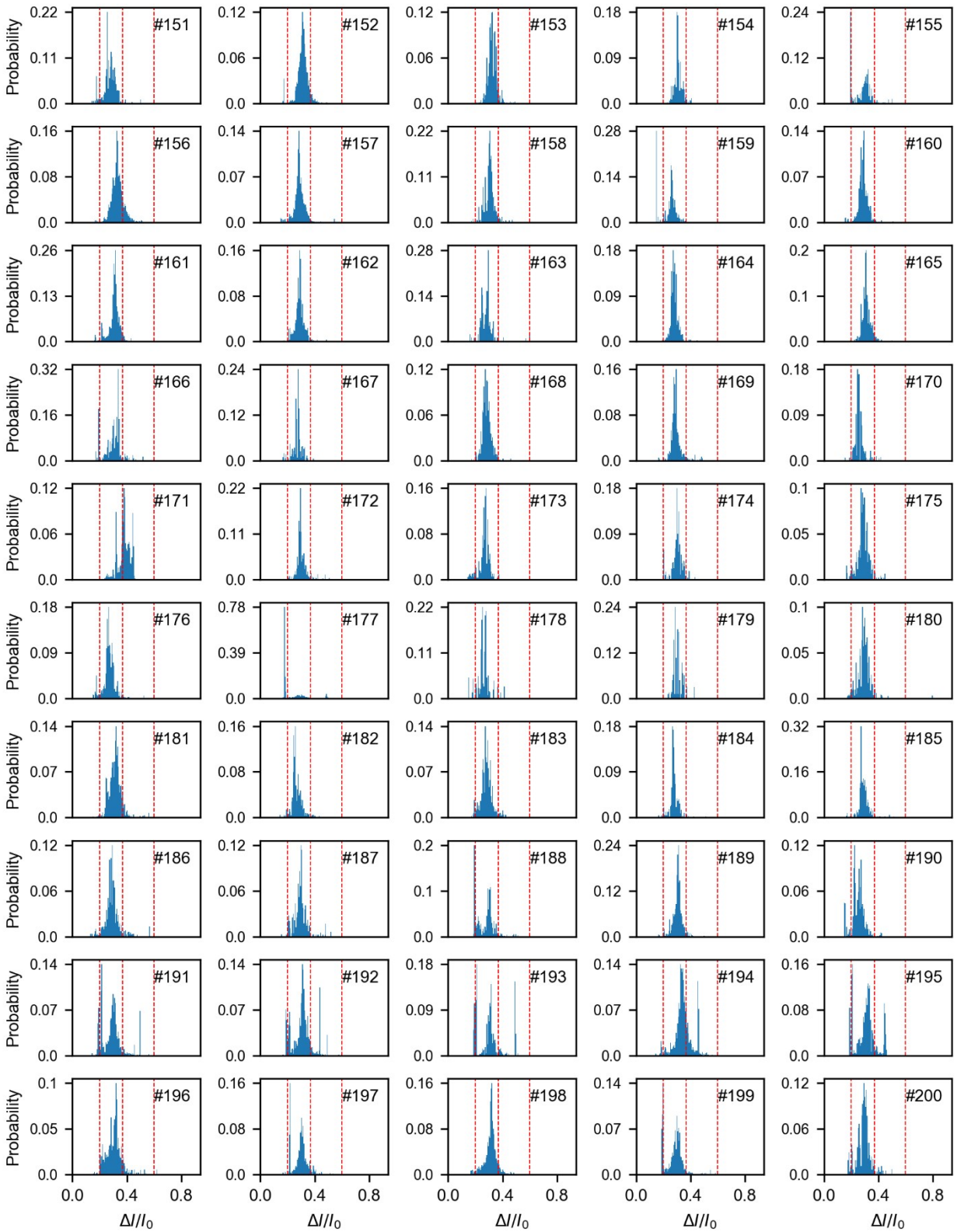


**Figure S28. The current histogram of single peptide events from event 151 to 200.** Each peptide produces the characteristic current distributions which could be divided into four stages by the dashed line with  $\Delta I/I_0 = 0.2, 0.37$  and  $0.6$  from left to right assigned as stage 1, stage 2, stage 3 and stage 4, respectively. All the data is acquired at  $+200$  mV in 1 M KCl, 10 mM Tris-HCL, pH 8.0 with a  $d \sim 4$  nm nanopore.

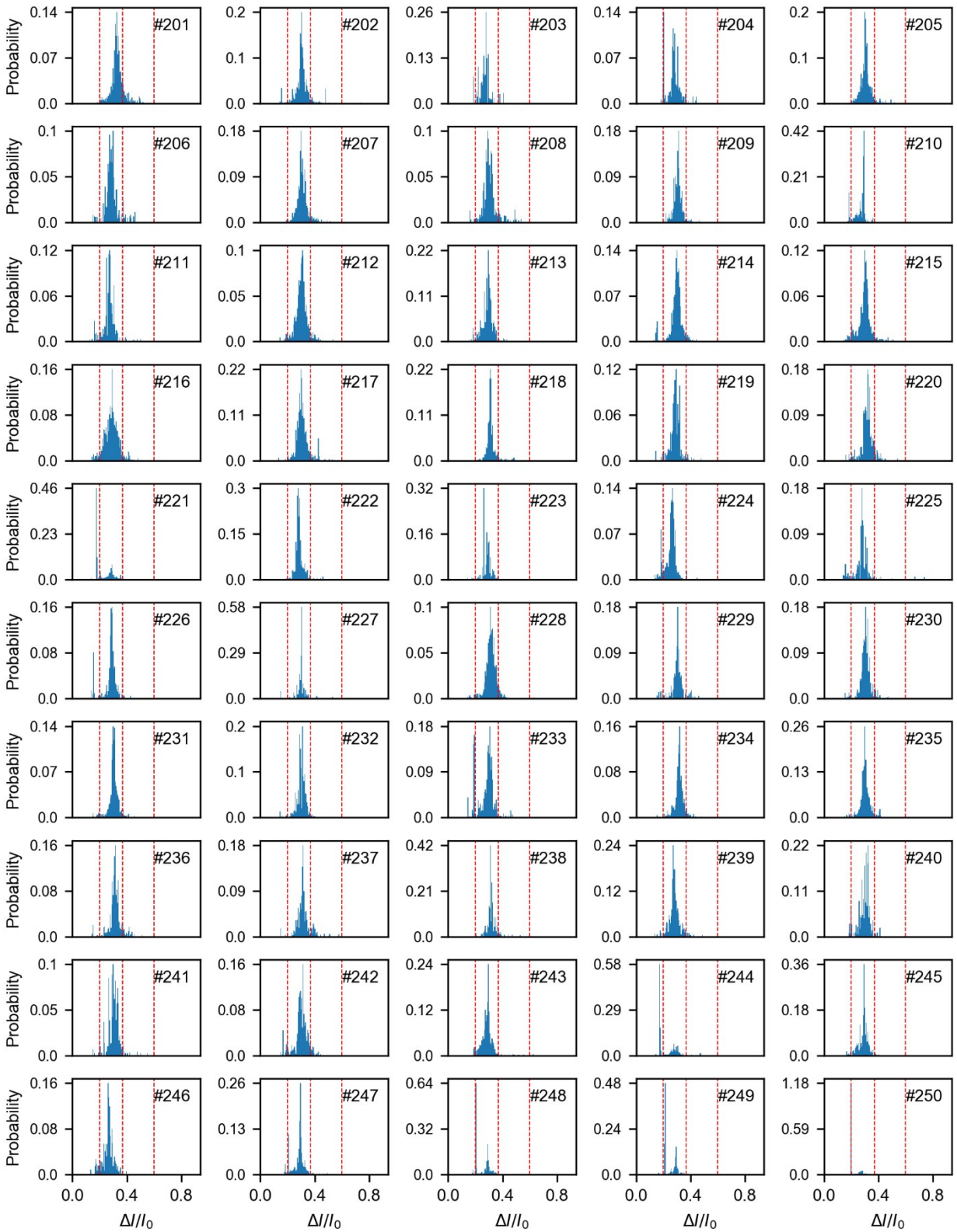


**Figure S29. The current histogram of single peptide events from event 201 to 250.** Each peptide produces the characteristic current distributions which could be divided into four stages by the dashed line with  $\Delta I/I_0 = 0.2, 0.37$  and  $0.6$  from left to right assigned as stage 1, stage 2, stage 3 and stage 4, respectively. All the data is acquired at  $+200$  mV in 1 M KCl, 10 mM Tris-HCL, pH 8.0 with a  $d \sim 4$  nm nanopore.

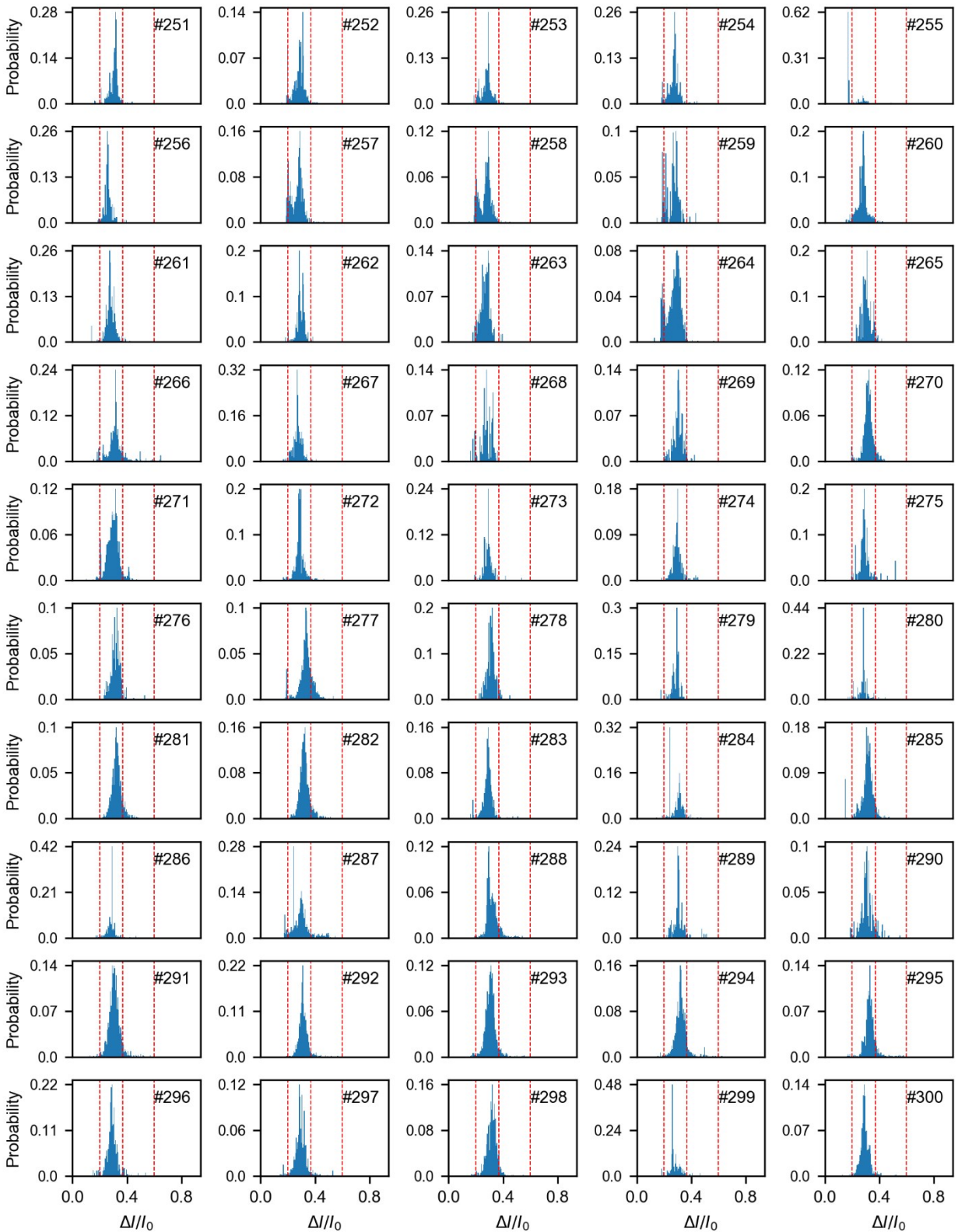


**Figure S30. The current histogram of single peptide events from event 251 to 300.** Each peptide produces the characteristic current distributions which could be divided into four stages by the dashed line with  $\Delta I/I_0 = 0.2, 0.37$  and  $0.6$  from left to right assigned as stage 1, stage 2, stage 3 and stage 4, respectively. All the data is acquired at  $+200$  mV in 1 M KCl, 10 mM Tris-HCL, pH 8.0 with a  $d \sim 4$  nm nanopore.

## 2.9 Current histogram of single peptide events with $d \sim 5$ nm nanopore under +50 mV.

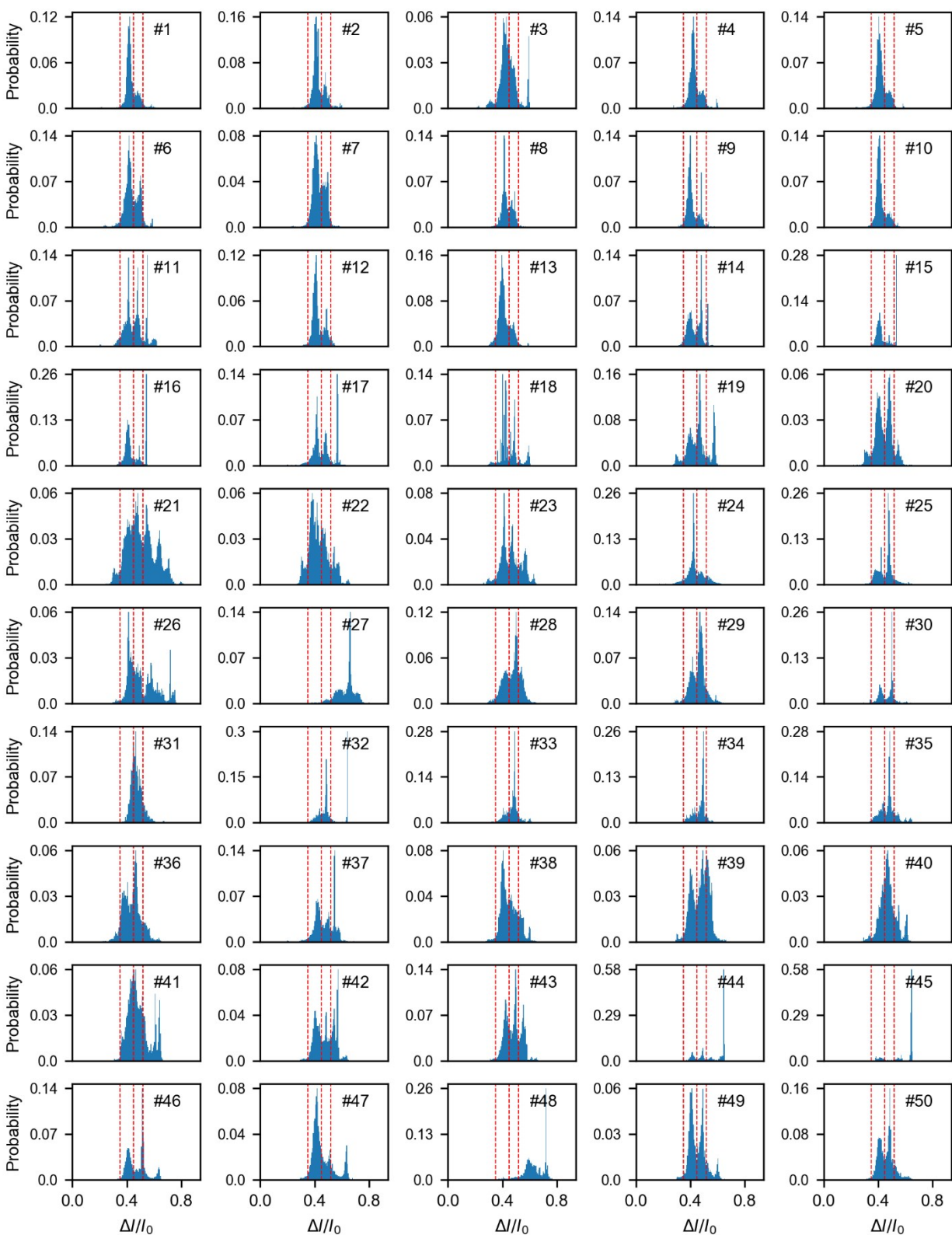


**Figure S31.** The current histogram of single peptide events from event 1 to 50. Each peptide produces the characteristic current distributions which could be divided into four stages by the dashed line with  $\Delta/I_0 = 0.35$ ,  $0.45$  and  $0.52$  from left to right assigned as stage 1, stage 2, stage 3 and stage 4, respectively. All the data is acquired at +50 mV in 1 M KCl, 10 mM Tris-HCl, pH 8.0 with a  $d \sim 5$  nm nanopore.

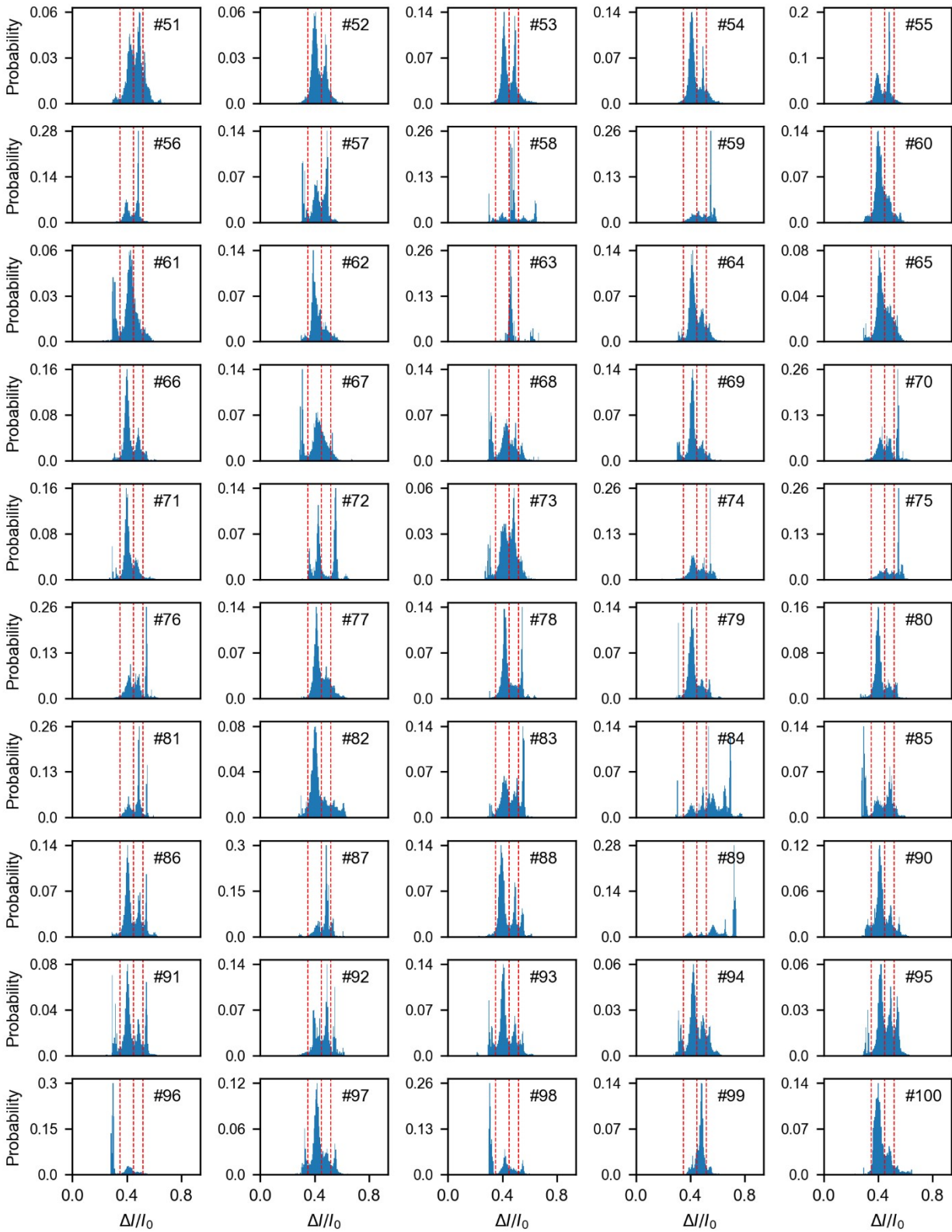


**Figure S32. The current histogram of single peptide events from event 51 to 100.** Each peptide produces the characteristic current distributions which could be divided into four stages by the dashed line with  $\Delta I/I_0 = 0.35, 0.45$  and  $0.52$  from left to right assigned as stage 1, stage 2, stage 3 and stage 4, respectively. All the data is acquired at  $+50$  mV in  $1$  M KCl,  $10$  mM Tris-HCl, pH 8.0 with a  $d \sim 5$  nm nanopore.

## 2.10 Current histogram of single peptide events with $d \sim 5$ nm nanopore under +100 mV.

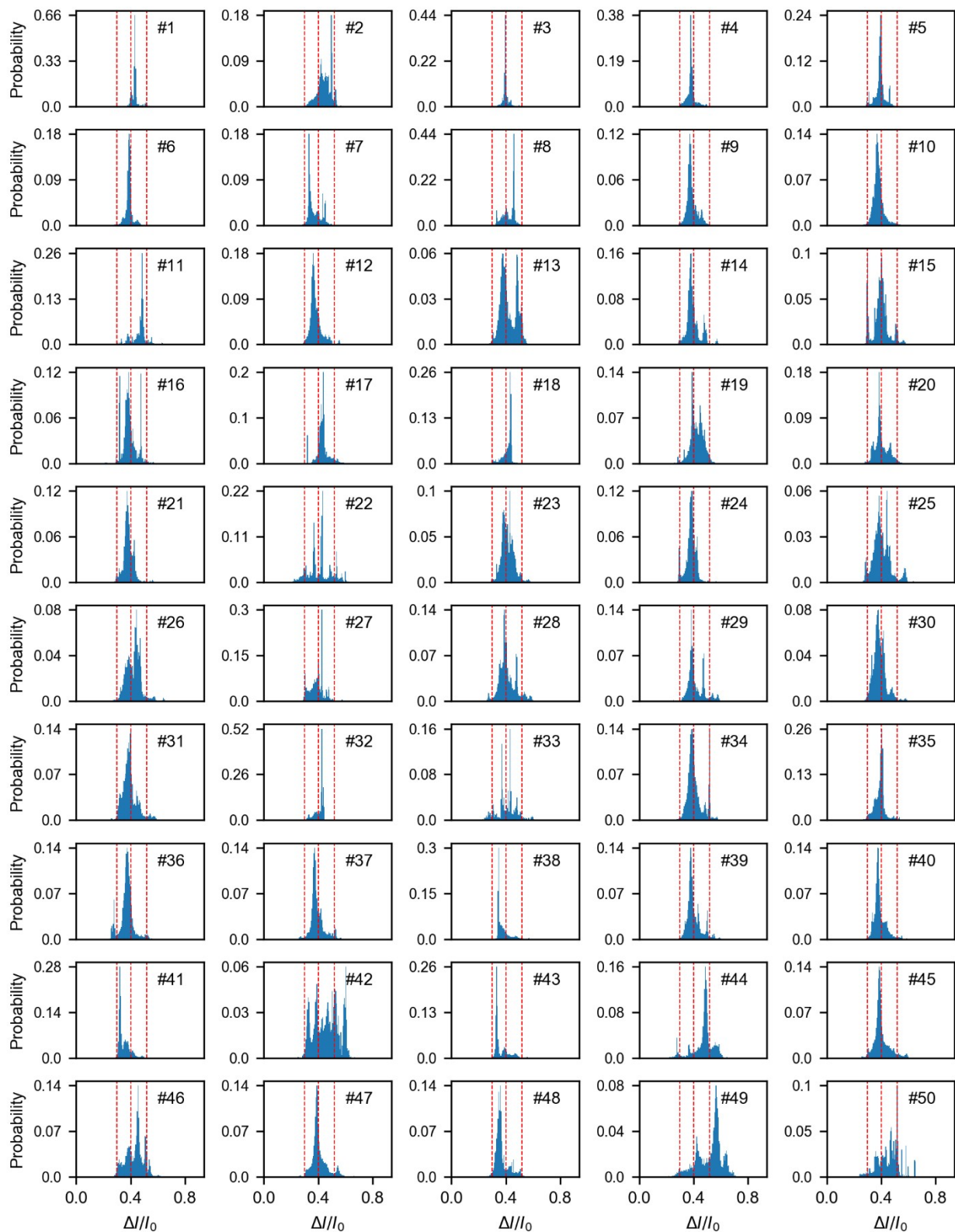


**Figure S33.** The current histogram of single peptide events from event 1 to 50. Each peptide produces the characteristic current distributions which could be divided into four stages by the dashed line with  $\Delta I/I_0 = 0.3, 0.4$  and  $0.52$  from left to right assigned as stage 1, stage 2, stage 3 and stage 4, respectively. All the data is acquired at +100 mV in 1 M KCl, 10 mM Tris-HCl, pH 8.0 with a  $d \sim 5$  nm nanopore.

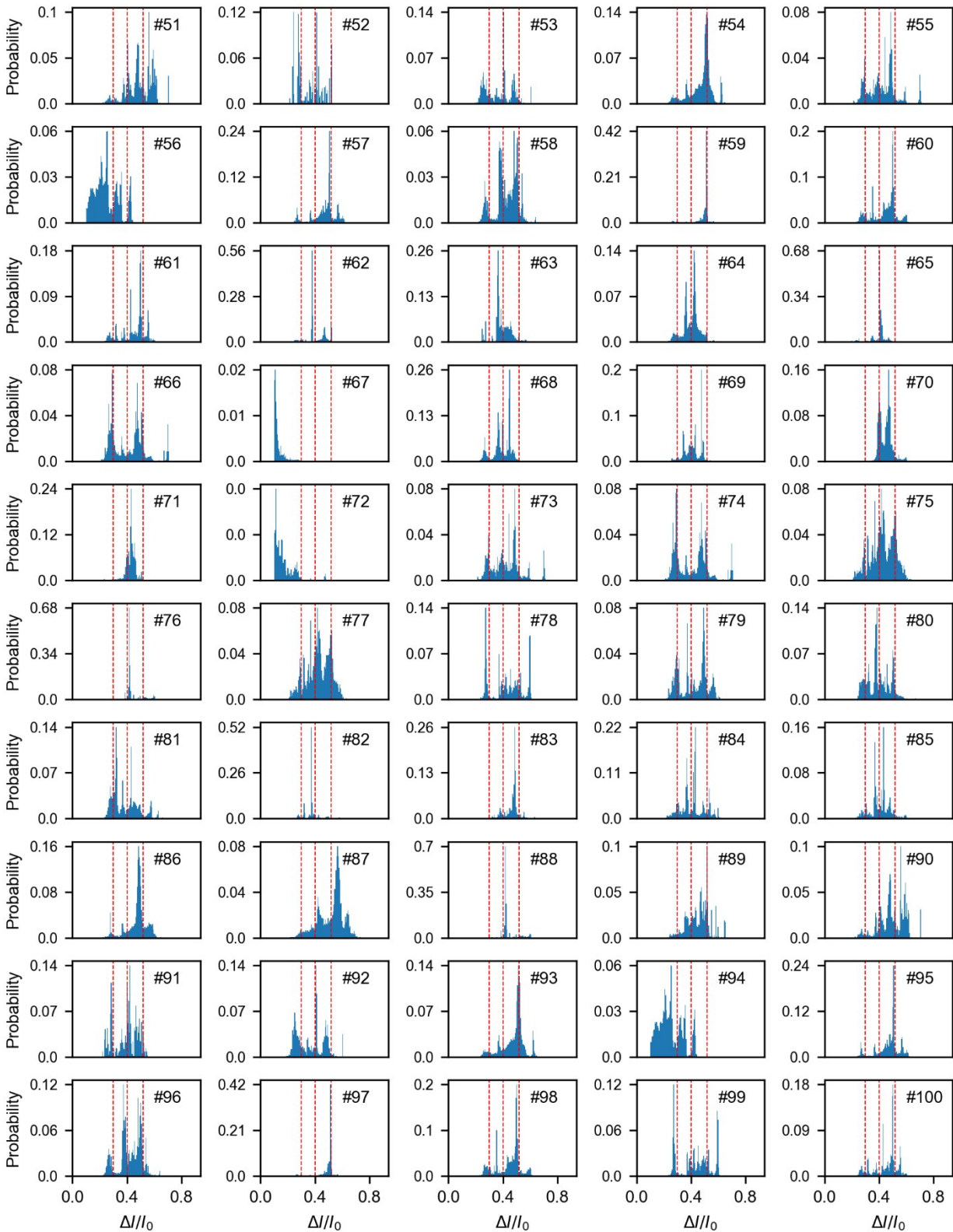


**Figure S34. The current histogram of single peptide events from event 51 to 100.** Each peptide produces the characteristic current distributions which could be divided into four stages by the dashed line with  $\Delta I/I_0 = 0.3, 0.4$  and  $0.52$  from left to right assigned as stage 1, stage 2, stage 3 and stage 4, respectively. All the data is acquired at  $+100$  mV in 1 M KCl, 10 mM Tris-HCL, pH 8.0 with a  $d \sim 5$  nm nanopore.



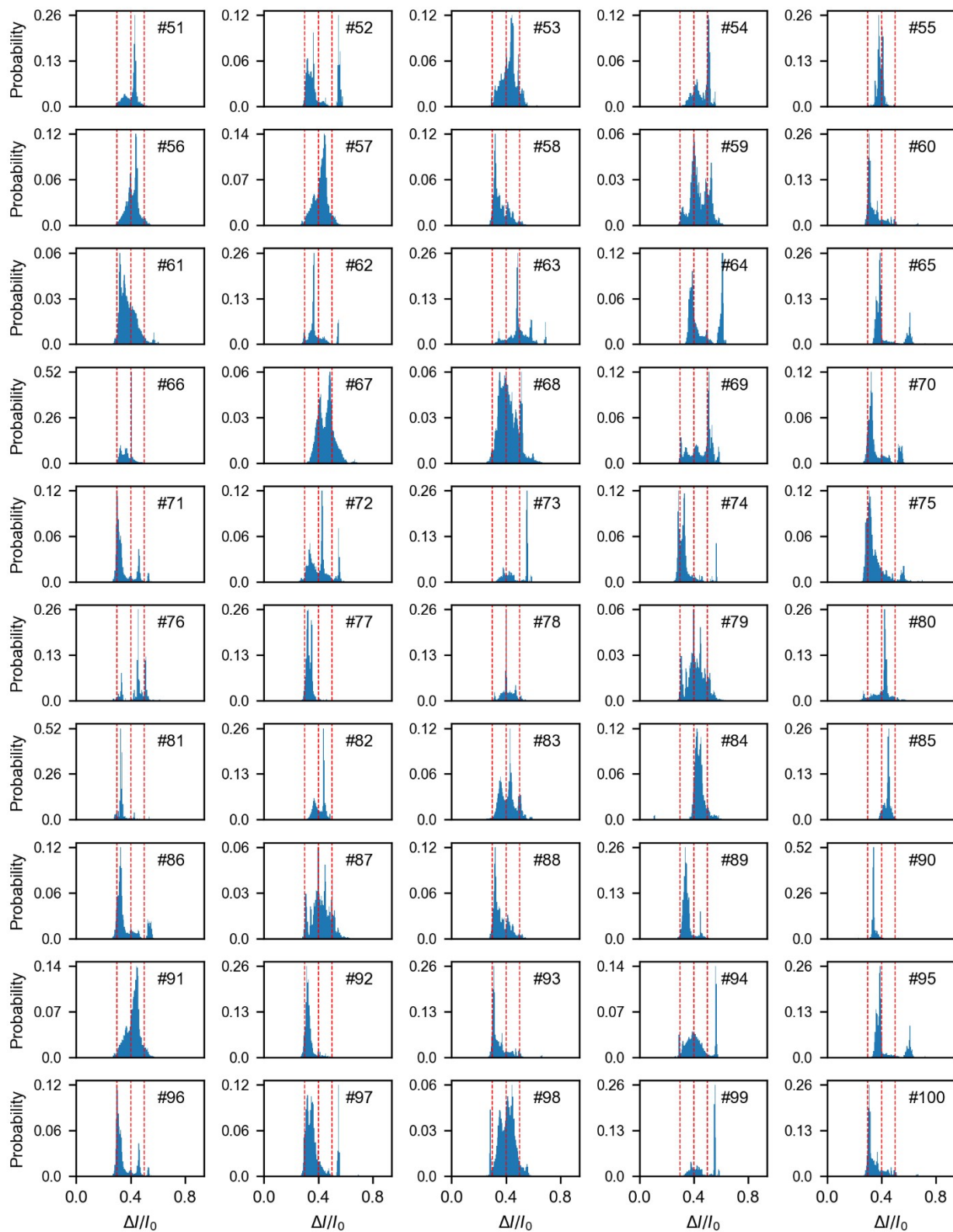


**Figure S36. The current histogram of single peptide events from event 51 to 100.** Each peptide produces the characteristic current distributions which could be divided into four stages by the dashed line with  $\Delta I/I_0 = 0.3, 0.4$  and  $0.5$  from left to right assigned as stage 1, stage 2, stage 3 and stage 4, respectively. All the data is acquired at  $+150$  mV in 1 M KCl, 10 mM Tris-HCL, pH 8.0 with a  $d \sim 5$  nm nanopore.

## References

- 1 Y. L. Ying and Y. T. Long, *Sci. China Chem.*, 2017, 60, 1187–1190.
- 2 Y. Lin, X. Shi, S.-C. Liu, Y.-L. Ying, Q. Li, R. Gao, F. Fathi, Y.-T. Long and H. Tian, *Chem. Commun.*, 2017, 53, 3539–3542.
- 3 H. Kwok, K. Briggs and V. Tabard-Cossa, *PLoS One*, 2014, 9, e92880.
- 4 S. W. Kowalczyk, A. Y. Grosberg, Y. Rabin and C. Dekker, *Nanotechnology*, 2011, 22, 315101.
- 5 I. Vodyanoy and S. M. Bezrukov, *Biophys. J.*, 1992, 62, 10–11.
- 6 I. Yanagi, R. Akahori, T. Hatano and K. I. Takeda, *Sci. Rep.*, 2015, 4, 5000.
- 7 Z. Gu, Y.-L. Ying, C. Cao, P. He and Y.-T. Long, *Anal. Chem.*, 2015, 87, 907–913.
- 8 Z. Gu, Y.-L. Ying, C. Cao, P. He and Y.-T. Long, *Anal. Chem.*, 2015, 87, 10653–10656.
- 9 PyNano, <https://decacent.github.io/PyNano>.
- 10 F. Biagini and M. Campanino, in *UNITEXT - La Matematica per il 3 piu 2*, 2016, vol. 98, pp. 81–87.
- 11 W. Humphrey, A. Dalke and K. Schulten, *J. Mol. Graph.*, 1996, 14, 33–38.
- 12 J. Eargle, D. Wright and Z. Luthey-Schulten, *Bioinformatics*, 2006, 22, 504–506.
- 13 E. Buckley, J. M. F. Alvarez, M. R. Smyth and R. O’Kennedy, *Electroanalysis*, 1991, 3, 43–47.